DEVELOPMENT OF METAL-DOPED ZINC FERRITE MAGNETIC SENSOR MATERIAL FROM STEEL DUST WASTE

TAN JIAN BIN

A project report submitted in partial fulfilment of the requirements for the award of Bachelor of Engineering (Honours) Mechanical Engineering

Lee Kong Chian Faculty of Engineering and Science
Universiti Tunku Abdul Rahman

May 2022

DECLARATION

I hereby declare that this project report is based on my original work except for citations and quotations which have been duly acknowledged. I also declare that it has not been previously and concurrently submitted for any other degree or award at UTAR or other institutions.

Signature : 

Name : TAN JIAN BIN

ID No. : 17UEB04046

Date : 15 May 2022

APPROVAL FOR SUBMISSION

I certify that this project report entitled **"DEVELOPMENT OF METAL-DOPED ZINC FERRITE MAGNETIC SENSOR MATERIAL FROM STEEL DUST WASTE"** was prepared by **TAN JIAN BIN** has met the required standard for submission in partial fulfilment of the requirements for the award of Bachelor of Engineering (Honours) Mechanical Engineering at Universiti Tunku Abdul Rahman.

Approved by,

Signature : 

Supervisor : DR. LEE HWANG SHENG

Date : 16 MAY 2022

Signature :

Co-Supervisor : NIL

Date :

The copyright of this report belongs to the author under the terms of the copyright Act 1987 as qualified by Intellectual Property Policy of Universiti Tunku Abdul Rahman. Due acknowledgement shall always be made of the use of any material contained in, or derived from, this report.

© 2022, TAN JIAN BIN. All right reserved.

ACKNOWLEDGMENTS

The project would not be accomplished without the assistance and contribution from few parties. Firstly, I would like to express my gratitude to my research supervisor, Dr. Lee Hwang Sheng for his invaluable advice, guidance throughout the research.

Special thanks to Universiti Tunku Abdul Rahman (UTAR), Lee Kong Chian Faculty of Engineering and Science - Department of Laboratory Management and Safety Administration (LKC FES-DLMSA), and Department of Mechanical and Material Engineering (DMME) for providing essential facilities, support and expertise for me during the process of completing this research project.

Last but not least, I would like to thank Nanotechnology & Catalysis Research Centre (NANOCAT) from the University of Malaya for their Vibrating Sample Magnetometer (VSM) testing service.

ABSTRACT

The steel dust, EAFD is a by-product from steel production. EAFD stands for electric-arc furnace dust. The amount of EAFD will continue to rise due to the growing demand for steel. The composition of the EAFD contains valuable metal elements, including Zn, Fe, Ca and Mn. Nevertheless, the EAFD is a hazardous solid waste due to its heavy metal elements. To date, researchers have managed to recover zinc from the EAFD through hydrometallurgical and pyrometallurgical processes. However, these processes produce waste. A different approach is required to transform the EAFD into a green product. Thus, the project's main aim is to develop the nickel zinc ferrite magnetic sensor material from the steel dust waste. Solid state reaction was applied to synthesize the Ni-Zn ferrite. The mixture of treated EAFD and nickel(II) chloride hexahydrate ($NiCl_2.6H_2O$) was sintered at 1100 °C for two hours with the mass ratio $R_{(TE/N)}$ of 6:4 and 8:2. The $R_{(TE/N)}$ is the mass ratio of treated EAFD to nickel(II) chloride hexahydrate. The synthesized Ni-Zn ferrite with the $R_{(TE/N)}$ of 6:4 has the magnetization (Ms) of 61.24 emu/g, coercivity (Hci) of 21.654 G, and retentivity (Mr) of 2.1941 emu/g. The synthesized nickel zinc ferrite with the $R_{(TE/N)}$ of 8:2 has Ms, Hci and Mr of 47.372 emu/g, 6.4347 G, and 0.57649 emu/g respectively. The Ni-Zn ferrite is a soft magnetic material. Hence, it can be used to develop magnetic sensors for high frequency applications (above 1MHz) in 5G technologies.

TABLE OF CONTENTS

LIST OF TABLES

LIST OF FIGURES

LIST OF SYMBOLS / ABBREVIATIONS

c_p	specific heat capacity, J/(kg·K)
h	height, m
K_d	discharge coefficient
M	mass flow rate, kg/s
P	pressure, kPa
P_b	back pressure, kPa
R	mass flow rate ratio
T	temperature, K
v	specific volume, m^3
α	homogeneous void fraction
η	pressure ratio
ρ	density, kg/m^3
ω	compressible flow parameter
ID	inner diameter, m
MAP	maximum allowable pressure, kPa
MAWP	maximum allowable working pressure, kPa
OD	outer diameter, m
RV	relief valve

CHAPTER 1

INTRODUCTION

1.1 General Introduction

There is no denying that a huge amount of steel dust will be produced during the manufacturing of the steel. The electric-arc furnace dust (EAFD) is the famous type of steel dust during the production of steel. It was reported that 10-20 kg of EAF dust will be produced for every 1 ton of steel from the electric arc furnace (EAF) smelting process (Wang, et al., 2020). Although there are a great variety of methods to produce steel, all of them have the same issue which is the generation of the steel dust waste (Moradpour, et al., 2020). In 2017, China already accounted for 0.7 million tons of EAF dust. The amount of EAF dust generated will continue to rise due to growing demand for steel (Wang, et al., 2020). The annual production of steel in Russia reported is approximately 20 Megatons, and 400000 tons of EAF dust was produced (Simonyan, Alpatova and Demidova, 2019). It was stated that Europe produced 158.8 million tonnes of crude steel in 2019. The specific amount and average amount of the by-products from the production of crude steel are shown in Table 1.1. BF represents the blast furnace whereas the BOF stands for basic oxygen furnace. BF and BOF are part of the iron ore-based steelmaking process (Rieger, et al., 2021).

Table 1.1: The Specific Amount and Average Amount of the By-products From the Production of Crude Steel (Rieger, et al., 2021).

Types of By-product	Specific Amount of By-product	Average Amount of By-product
BF slag	150 - 347 kg/t hot metal (HM)	249 kg/t HM
BF dust	3 - 18 kg/t HM	11 kg/t HM
BF sludge	2 - 22 kg/t HM	12 kg/t HM
Desulphurization slag	3 - 40 kg/t liquid steel (LS)	125 kg/t LS
BOF slag	85 - 165 kg/t LS	13 kg/t LS
BOF dust	1 - 24 kg/t LS	16 kg/t LS
BOF sludge	15 - 16 kg/t LS	165 kg/t LS
EAF slag	60 - 270 kg/t LS	20 kg/t LS
EAF dust	10 - 30 kg/t LS	45 kg/t LS
Ladle furnace slag	10 - 80 kg/t LS	5 kg/t LS
Mill scale	2 - 8 kg/t LS	

The World Steel Association stated that the slag (90% by mass), sludge and dust are the main solid co-products of the iron and crude steel production (World Steel Association, 2018). In 2010, it was reported that an average outputs of 1 tonne of crude steel produced 200 kg (EAF route) to 400 kg (BF/BOF route) of co-products as shown in Figure 1.1.

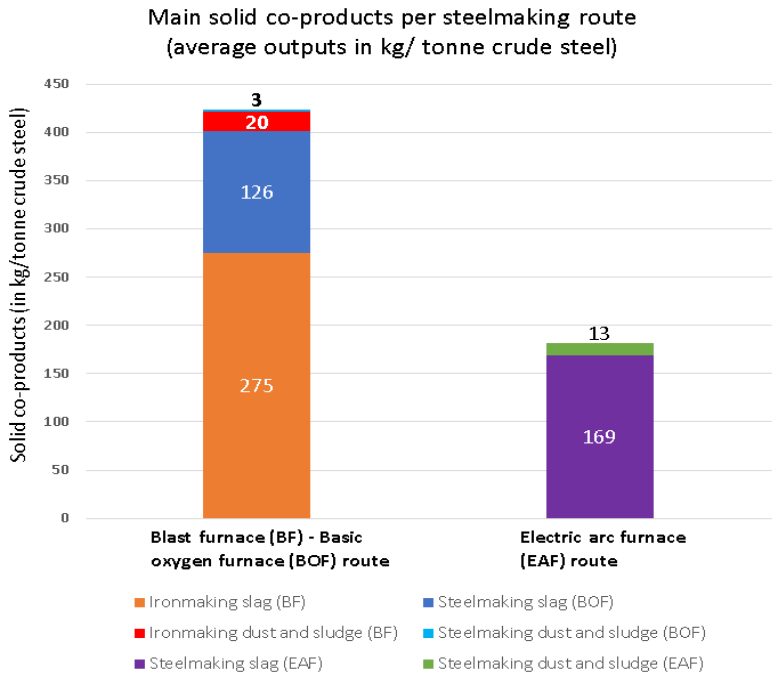

Figure 1.1: Main Solid Co-products Per Steelmaling Route Bar Chart in 2010 (World Steel Association, 2018).

The composition of the EAF dust contains several valuable metal elements such as calcium (Ca), zinc (Zn), iron (Fe) and manganese (Mn). Nevertheless, the United States Environmental Protection Agency categorized the EAF dust as a hazardous solid waste. This is due to the presence of the heavy metal elements such as cadmium (Cd), chromium (Cr), and lead (Pb) (Wang, et al., 2020). These three hazardous elements are harmful to human health and the environment.

To date, actions have been implemented to recover the valuable metal elements (e.g. iron and zinc) from the EAF dust especially with hydrometallurgical and pyrometallurgical processes. Apart from the recovery of the valuable elements from the dust, incorporation of the dust waste into other materials has been implemented. This means that the dust waste can be used as a raw material of a product which can prevent the hazardous element released into the environment (de Buzin, Heck and Vilela, 2017). Nevertheless, there is not much research and studies on the utilization of the steel dust to produce green products yet (Wang, et al., 2017).

With the composition of the EAF dust as mentioned above, it is possible to make use of the dust as a raw material to synthesise spinel ferrite.

For example, nickel zinc spinel ferrite is a mixed spinel ferrite, which has low coercivity and high saturation magnetization. Thus, it is famously used in the application of high frequency soft magnetic ferrite. There is an increasing demand for the nickel zinc spinel ferrite material due to its magnetic properties (Wang, et al., 2020). Generally, the nickel zinc spinel ferrite is prepared with pure reagents. In other works, zinc bearing electric arc furnace dust (ZEAFD) with the addition of nickel (II) hydroxide were used to prepare nickel zinc spinel ferrite nanopowder by solid state reaction. Its magnetic properties were evaluated and it was reported that the prepared spinel ferrite has saturation magnetization of 57.3 emu/g as well as the coercivity of 58.8 Oe. A toxicity assessment was performed to evaluate the synthesised spinel ferrite and the result showed that the spinel ferrite was not toxic (green product) (Wang, et al., 2020). Besides, similar work was conducted by using the zinc bearing dust from a stainless steel plant as a raw material to prepare a Ni-substituted ferrite. The solid state reaction technique was used to synthesise the Ni-substituted ferrite. It was reported that the level of the hazardous heavy metal elements in the synthesised spinel ferrite sample was below the maximum limit. The hysteresis loop data of the prepared Ni-substituted ferrite showed that it has a saturation magnetization of 47.6 emu/g as well as a coercivity of 98 Oe (Gao and Cheng, 2018). Therefore, in this project, the investigation regarding the development of nickel-doped zinc ferrite magnetic sensor material from the steel dust will be performed.

1.2 Importance of the Study

The outcome of this study may provide new idea regarding the alternative methods to recycle or treat the steel dust waste. There were many studies on the recovery of valuable elements such as zinc, Zn from the steel dust by pyrometallurgical process, hydrometallurgical process, carbothermic reduction method, and hydrothermal method. In this study, the steel dust will be utilised as a raw material to develop the nickel-doped zinc ferrite magnetic sensor. Hence, this study may promote the idea of using the steel waste as a raw material to manufacture the nickel zinc ferrite material in the industry. It is hoped that this study can encourage the industries that manufacture ferrite materials to

make use of the steel dust for their benefit as well as reducing the steel dust pollution to the environment.

1.3 Problem Statement

The electric-arc furnace dust (EAFD) is the byproduct of the steel production. The steel dust contains hazardous elements including lead, chromium, as well as cadmium. Many research studies were conducted to develop approaches to treat or recycle the steel dust. The valuable metal elements of the steel dust such as iron and zinc can be recovered instead of being treated as waste (Wang, et al., 2016). However, to date, more focus has been put on the hydrometallurgical and pyrometallurgical processes for zinc recovery from the steel dust. The pyrometallurgical process which is the widely used commercial method in the industry has a few drawbacks. For instance, it produces a significant amount of worthless waste. In Spain, an approximate of 56 percent of the processed waste which require proper disposal methods are generated from the pyrometallurgical process in treating the EAF dust. Also, the dioxin which is highly toxic will be generated during the pyrometallurgical process (de Buzin, Heck and Vilela, 2017). Besides, the hydrometallurgical process has several disadvantages such as the loss of the valuable reagents and the huge amount of untreated wastewater from the washing process (de Buzin, Heck and Vilela, 2017). Thus, a different solution is required to transform the steel dust or EAF dust into another product such as the magnetic spinel ferrite without causing pollution (green product). In this paper, a nickel doped zinc ferrite magnetic sensor will be prepared from the EAF dust.

The steel dust or EAF dust is hazardous due to the presence of the hazardous element such as chromium, cadmium and lead. The synthesised nickel-doped zinc ferrite magnetic sensor should not have any hazardous elements in its composition. Otherwise, the quality of the nickel-doped zinc ferrite magnetic sensor will be affected detrimentally.

Wang, et al. (2020) performed the toxicity characteristic leaching procedure (TCLP) to evaluate the toxicity of the samples. The toxicity assessment indicated that the concentrations of lead, chromium, nickel and zinc from the washed sample were below the limit of detection. This means that the synthesized nickel zinc ferrite with washing treatment is non-toxic. Lead is

hazardous and the synthesized nickel zinc ferrite still has a small amount of lead element within its compound. To date, there is no study on the long term effect of the lead element within the compound of the synthesized nickel zinc ferrite (Wang, et al., 2020).

1.4 Aim and Objectives

The main aim of this study is to develop the metal doped zinc ferrite magnetic sensor material from steel dust waste instead of using pure chemical reagents. Hence, the objectives of this study are shown below:

- To analyse the chemical composition of the EAFD and the synthesized nickel doped zinc ferrite.
- To synthesize nickel doped zinc ferrite magnetic sensor material from the EAFD.
- To evaluate the magnetic properties of the synthesized Ni-Zn ferrite such as the magnetic saturation and coercivity by Vibrating Sample Magnetometer (VSM).

1.5 Scope of the Study

The scope of study in this project involves the synthesis of nickel-doped zinc ferrite by solid state reaction technique. The EAFD will be treated with diluted hydrochloric acid solution before it is mixed with the nickel(II) chloride hexahydrate to synthesize nickel-doped zinc ferrite samples. The effect of different mass ratio, $R_{(TE/N)}$ of treated EAFD to nickel(II) chloride hexahydrate on the magnetic performance of the synthesized nickel-doped zinc ferrite samples will be evaluated. The magnetic performance of the synthesized samples will be determined with the Vibrating Sample Magnetometer (VSM). Furthermore, the characterizations of the synthesized nickel-doped zinc ferrite will be evaluated with the Scanning Electron Microscopy with Energy Dispersive X-Ray (SEM-EDX), X-ray Diffraction (XRD), and Fourier Transform Infrared Spectroscopy (FTIR) analysis.

CHAPTER 2

LITERATURE REVIEW

2.1 Introduction of Electric-arc Furnace Dust (EAFD)

Based on the statistics data of the world crude steel production from Steel Statistical Yearbook 2018, the amount of crude steel production was 1690.5 million tons worldwide in the year of 2017. Figure 2.1 shows that China accounted for the most production of the crude steel in 2017 which was 49.2 % as compared to other countries. The crude steel production in Europe (12.6 %) was greater than that of the USA, Japan and India in 2017 (Xiaobin, et al., 2021).

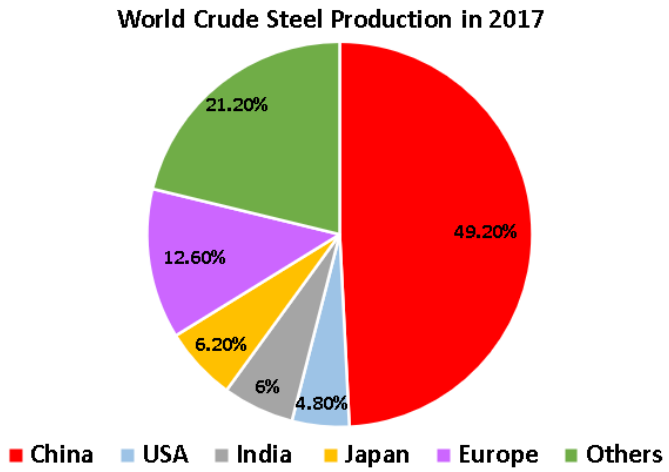

Figure 2.1: The Data of World Crude Steel Production in 2017 (Xiaobin, et al., 2021).

Most of the semi-integrated mills and mini-mills which were commonly used in the steel production have an electric melting shop. The electric-arc furnace as shown in Figure 2.2 is employed in the electric melting shop as scrap melting equipment. The vaporization of nonferrous metals with the molten iron, the bursting of the carbon monoxide bubbles, as well as the ejection of particles from the metal liquid bath result in the generation of the electric-arc furnace dust (EAFD) during the steel production (de Buzin, Heck and Vilela, 2017).

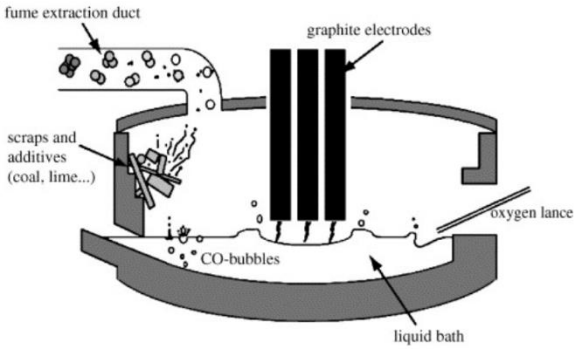

Figure 2.2: The Schematuic Diagram of Electric Arc Furnace (Guézennec, et al., 2005).

The electric-arc furnace dust (EAFD) or commonly known as the steel dust is one of the byproducts from the steel production. It was stated that when the amount of steel manufactured is 1 ton, it will contribute to the discharge of 12-14 kg of steel dust or EAF dust. In 2009, it was declared that the USA alone had generated 0.9 million tons of EAF dust. Then in 2014, the amount of EAF dust generated in China was 0.1 million tons (Wang, et al., 2017). Besides, the production of the EAF dust worldwide will reach an approximate of 3.7 million tons every year and it will continue to rise annually by 4 - 6 percent (Moradpour, et al., 2020).

The US Environmental Protection Agency claimed that the EAF dust is categorised as a hazardous solid waste. This is mainly due to the presence of lead (Pb), chromium (Cr), and cadmium (Cd) within the dust (Wang, et al., 2017). The lead and cadmium are classified as heavy metals which are harmful to human health and environment. Thus, many countries consider this dust as a hazardous waste (de Buzin, Heck and Vilela, 2017). Nevertheless, the steel dust does contain valuable elements. For instance, zinc (Zn), iron (Fe), calcium (Ca), manganese (Mn), etc (Wang, et al., 2017). Today, many studies and efforts have been implemented to study the best approach to regain these elements from the dust. Generally, the pyrometallurgical and hydrometallurgical methods were implemented to regain the valuable elements from the EAF dust (Wang, et al., 2017).

2.2 Electric-arc Furnace Dust (EAFD) Treatment

The EAF dust is hazardous due to the presence of lead (Pb), chromium (Cr), and cadmium (Cd) within the dust (Wang, et al., 2017). However, the EAF dust contains valuable zinc and iron elements. There are several types of processes to recover the zinc from the dust. They are hydrometallurgical processes, high temperature metal recovery processes (HTMR), as well as hybrid process. To date, the HTMR processes still account for the major zinc recovery from the EAF dust process. Based on a few studies, the lead from the EAF dust was reported that it will volatilize in the form of lead chloride, $PbCl_2$ during the HTMR processes. The reaction of lead oxide (PbO) with the chlorides such as sodium chloride and potassium chloride which are within the dust results in the formation of lead chloride. Yoo, et al. (2005) stated that when the lead and chlorine are removed from the EAF dust, the zinc loss needs to be minimized to ensure high purity zinc recovery during HTMR processes. Yoo, et al. (2005) conducted a study to investigate the volatilization of Pb from the EAF dust at the temperature ranging from 973 to 1223 K in air. The lead's volatilization reaction in this study was $2NaCl + PbO + 2SiO_2 + Al_2O_3 = PbCl_2(g) + 2NaAlSiO_4$. The study showed that when the reaction took place at 1223 K for 90 minutes, approximately 98% for chlorine and lead were volatilized whereas there was approximately 1% of zinc loss. Solid-state diffusion was utilised to control the volatilization of Pb. Thus, this study proved that it is possible to remove lead and chlorine while reducing the zinc loss from the dust during the zinc recovery processes (Yoo, et al., 2005).

Nezhad and Zabett (2016) conducted a study on the thermodynamic analysis of zinc recovery from the EAF dust by using the carbon and ferrosilicon. In this study, a pretreatment process was performed before the zinc recovery process. The purpose of the pretreatment process was to eliminate the volatile compounds from the EAF dust which can prevent impurities in the final product. An electric furnace was used to heat 100 grams of EAF dust in an alumina boat. The heating process was conducted for 4 hours. After that, the dust sample was cooled in the furnace to room temperature. Table 2.1 shows the element composition of the EAF dust used in the study. Nezhad and Zabett (2016) stated that due to the presence of the carbon element (2.1 %) in the dust, the amount of zinc loss will be increased during the pretreatment process.

Table 2.1: The Chemical Composition of the EAF Dust (Nezhad and Zabett, 2016).

Element	Fe	Zn	Ca	Pb	Na	Mg	Al	Cd	Cr
wt%	30.0	19.02	4.5	0.99	3.38	4.99	0.53	0.04	0.34
Element	K	Si	C	Cl					
wt%	0.16	0.16	2.1	6.45					

Based on Figure 2.3, the graph shows that when the temperature rised, the amount of zinc loss increased during the pretreatment process. To prevent significant zinc loss, the pretreatment of the dust should be performed at a temperature lower than 900 °C.

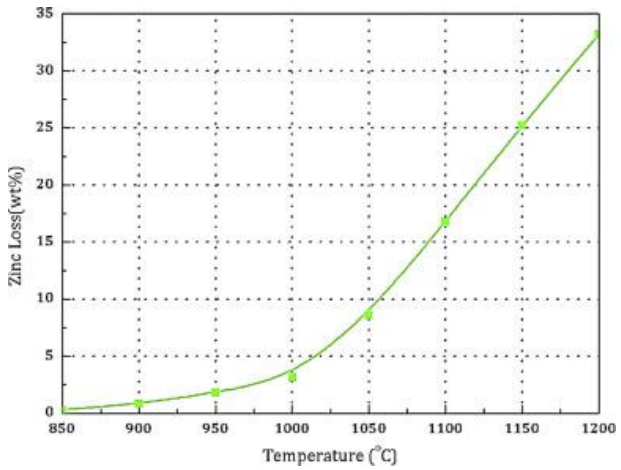

Figure 2.3: The Amount of Zinc Loss (wt%) Versus Temperature During the Pretreatment of EAFD (Nezhad and Zabett, 2016).

The graph as shown in Figure 2.4 was plotted to determine the suitable temperature to remove the volatile elements in the EAF dust. The graph of number of moles of air needed to achieve 95% removal of potassium, cadmium and lead from 850 °C to 900 °C was plotted as shown in Figure 2.4. At 875 °C, the number of moles of air to remove ninety-five percents of volatile potassium, cadmium and lead are 93, 73 and 108 respectively as shown in Figure 2.4.

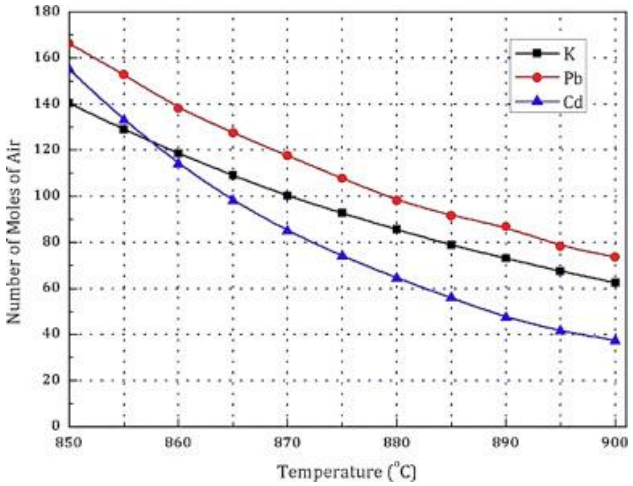

Figure 2.4: The Number of Moles of Air Required for 95% Removal of Volatile Elements (K, Pb and Cd) During the Pretreatment Process (Nezhad and Zabett, 2016).

Chairaksa-Fujimoto, et al. (2016) conducted a study on the selective leaching of zinc oxide from Electric Arc Furnace dust which was pretreated with calcium oxide. The sodium hydroxide (NaOH) solution was used for the leaching process. The pretreatment process was conducted at a temperature of either 900 °C or 1100 °C for less than 3 hours. The purpose of the pretreatment process with calcium oxide (CaO) was to convert the zinc ferrite ($ZnFe_2O_4$) in the EAF dust to zinc oxide (ZnO) and calcium ferrite ($Ca_2Fe_2O_5$) without carbothermic reduction. This is because the $ZnFe_2O_4$ in the EAF dust cannot dissolve easily in aqueous solutions. Thus, the ZnO that was resulted from the CaO pretreatment process can dissolve in either alkaline or acidic solutions for zinc leaching process. The zinc can be recovered from the CaO treated EAF dust. In addition, the pretreatment process by using the CaO also helped to remove the heavy metals, fluoride and chloride elements without the loss of iron and zinc through evaporation. Therefore, it was stated that the pretreated dust does not contain heavy metals, fluoride or chloride elements (Chairaksa-Fujimoto, et al., 2016).

Wang, et al. (2020) utilized nickel (II) hydroxide ($Ni(OH)_2$) and Zn-bearing EAFD to obtain the nickel-zinc ferrite nanopowder, $(Ni,Zn)Fe_2O_4$ by solid state calcination approach. The Scanning Electron Microscopy (SEM) and Energy Dispersive Spectroscopy (EDS) were utilised to analyse surface morphologies as well as the chemical compositions of the calcined sample and

the washed sample respectively. The washed sample had been washed with dilute acetic acid (Hac) solution after the calcination process. The purpose of the washing procedure was to remove the metal elements that did not remain in the synthesized ferrite. Based on the EDS data as shown in Figure 2.5, it is shown that the chemical composition of Cl, Na and K elements from the washed sample are significantly lower than that of the calcined sample.

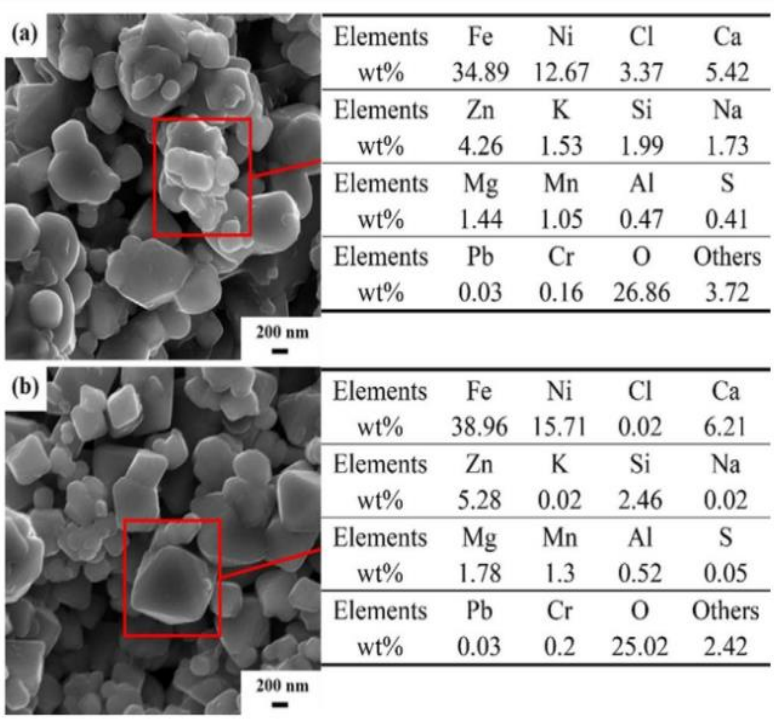

Elements	Fe	Ni	Cl	Ca
wt%	34.89	12.67	3.37	5.42
Elements	Zn	K	Si	Na
wt%	4.26	1.53	1.99	1.73
Elements	Mg	Mn	Al	S
wt%	1.44	1.05	0.47	0.41
Elements	Pb	Cr	O	Others
wt%	0.03	0.16	26.86	3.72

Elements	Fe	Ni	Cl	Ca
wt%	38.96	15.71	0.02	6.21
Elements	Zn	K	Si	Na
wt%	5.28	0.02	2.46	0.02
Elements	Mg	Mn	Al	S
wt%	1.78	1.3	0.52	0.05
Elements	Pb	Cr	O	Others
wt%	0.03	0.2	25.02	2.42

Figure 2.5: The EDS Analysis on The Composition of (a) The Calcined Sample and (b) the Washed Sample (Wang, et al., 2020).

2.3 Introduction of Spinel Ferrite

The spinel ferrite has the general formula of MFe_2O_4. The M of the MFe_2O_4 formula represents the divalent ions which is generally known as Ni^{2+}, Mn^{2+}, Zn^{2+}, Co^{2+}, Mg^{2+}, etc (Qin, et al., 2021). The spinel ferrite is famous for its stability, microwave, dielectric, electrical, and magnetic properties. Thus, they are amazingly suitable for a vast range of applications including catalysts, energy storage, biomedicines, biosensors, electromagnetic interference shielding, ferrofluid, wastewater treatment and magnetic media (Tsay, Chiu and Tseng, 2019).

Another basic formula of the spinel ferrites is known as $Me_{\alpha}^{2+}Fe_{1-\alpha}^{3+}[Me_{1-\alpha}^{2+}Fe_{1+\alpha}^{3+}]O_4^{2-}$. Me represents the metal ion. The spinel ferrites is then categorized into three groups according to the **α** value. The three groups are normal spinel structure, inverse spinel structure and mixed spinel structure (Kaur and Bhargava, 2021).

In the normal spinel structure, the **α** value is 1 which results in the basic formula of $Me^{2+}Fe_2^{3+}O_4^{2-}$. The divalent cations occupy all eight tetrahedral sites while the trivalent cations occupy all sixteen octahedral sites of the normal spinel structure. One of the common examples of the normal spinel structure is zinc ferrite ($ZnFe_2O_4$) (Kaur and Bhargava, 2021).

The **α** value is 0 in the inverse spinel structure. Hence, $Fe^{3+}[Me^{2+}Fe^{3+}]O_4^{2-}$ is its basic formula. All its divalent cations are located at the octahedral sites only. The amount of the trivalent cations are separated equally between the tetrahedral and octahedral sites. The nickel ferrite is an inverse spinel structure (Kaur and Bhargava, 2021).

The **α** value of the mixed spinel structure lies between zero and one. It has the basic formula of $Me_{1-\alpha}^{2+}Fe_{\alpha}^{3+}[Me_{\alpha}^{2+}Fe_{2-\alpha}^{3+}]O_4^{2-}$. Its divalent and trivalent cations exist in both tetrahedral and octahedral sites. The nickel zinc ferrite is a popular mixed spinel ferrite. The Ni-Zn ferrite has the formula of $Fe_{1-\alpha}^{3+}Zn_{\alpha}^{2+}[Fe_{1+\alpha}^{3+}Ni_{1-\alpha}^{2+}]O_4^{2-}$ (Kaur and Bhargava, 2021).

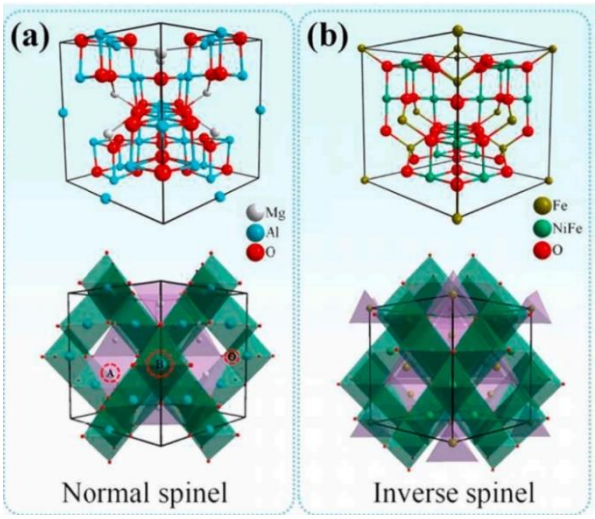

Figure 2.6: Structure of Normal Spinel and Inverse Spinel (Qin, et al., 2021).

2.4 Application of Ni-Zn Ferrites as Magnetic Sensor

The nickel zinc ferrite $(Ni,Zn)Fe_2O_4$ will be studied in this paper due to several reasons. One of the reasons is that the nickel zinc ferrite is a type of a soft magnetic material. Therefore, it exhibits low coercivity (Hc) with high magnetic saturation (Ms). In addition, the nickel zinc ferrite has other attractive properties such as high dielectric, high permeability, high resistivity, high mechanical strength as well as low power loss (Kaur and Bhargava, 2021). The nickel zinc ferrite has captured global industry attention due to its properties. There is a great variety of applications for the nickel zinc ferrite material. For instance, it can be utilised in the field of permanent magnets, antenna rods, devices for telecommunication, magnetic refrigeration, catalyst, sensors, etc (Džunuzović, et al., 2015).

The development of the nickel zinc ferrite magnetic sensor will be studied in this project. Many types of sensors have been developed for different applications such as building security, air circulation control of the building, temperature and humidity control of the housing, sensors for motor vehicles, etc. Based on the information from the IC Insights 2017, it was declared that all the categories of the sensors such as magnetic sensors, acceleration sensors as well as the pressure sensors had achieved two-digit sales in 2016. It was estimated that the market of the sensors would rise by 7.8 percent and reach a record of USD 12.8 billion in 2017. In addition, there are several contributing factors that will drive the sales of the market sensors. For instance, the increasing demands of robotics in the manufacturing industry, unmanned aircraft for military purposes, high tech electronic gadgets (e.g. smartphone, laptop, camera, etc), and automated control functions (e.g. autonomous vehicles). Therefore, the growing demands of the magnetic sensors has driven the researches as well as studies on the magnetic sensors recently. The magnetic sensors have a vital impact in a great variety of applications such as automotive sensors, magnetic storage, security system, navigation system, and medical sensors (Asfour, 2017).

Based on the magnetic properties of the nickel zinc ferrite materials as mentioned above, the nickel zinc ferrite which is considered as a soft ferrite can be used to develop a magnetic sensor. The volume resistivity (ρ) of the nickel zinc ferrite material ranges from several kiloohm-centimeter (kOhm-cm) to tens

of megaohm-centimeter (MOhm-cm). Generally, the nickel zinc ferrite magnetic sensor is suitable for the high frequency applications which are above 1 MHz. Also, it can be utilised for low flux density applications. For instance, antenna, transformer, EMI (electromagnetic interference) suppression, and broadband RF (radio frequency) (Fair-Rite Products Corp., 2021).

According to 10-10 Malaysian Science, Technology, Innovation and Economy (Mystie) Framework, it stated that the agriculture and forestry sector play vital role in the generating employments and economic wealth for the nation. However, the agriculture and forestry sector in Malaysia is more towards labour-intensive instead of technology-driven. Consequently, Malaysia has to rely on foreign countries to meet the demanding agro-food requirements. The framework suggested that technologies can be utilised to transition or facilitate the sector to more technology-intensive. For instance, 4G/5G network, sensor technology, and bioscience technology can be applied to modernise the sector. These technologies require magnetic sensor. Besides, modernising the agriculture and forestry sector will drive the economy or market of other sectors such as smart cities and transportation, medical and healthcare, engineering and manufacturing, business and financial services, as well as education. The demand of the magnetic sensor in Malaysia will rise (Academy of Sciences Malaysia, 2020). Hence, the nickel zinc ferrite which is synthesized from the electric arc furnace dust (EAFD) can be the potential alternative to the nickel zinc ferrite magnetic sensor that is manufactured with pure reagents.

2.5 Synthesis of Ni-Zn Ferrite by Solid State Reaction from Pure Reagents and EAF Dust

There are a couple of methods to synthesise the nickel zinc ferrite with pure reagents. Chemical type method is widely utilised to synthesise spinel ferrite such as sol-gel auto combustion, solid state reaction, hydrothermal method, and co-precipitation (Qin, et al., 2021).

In this project, the solid state reaction will be utilised to synthesise the nickel zinc ferrite. The nickel zinc ferrite also can be synthesised from the pure reagents by solid state reaction. The solid state reaction is also known as the conventional ceramic method. This technique is chosen in this study due to its starting materials being cheap and its availability in the industry. Also, the solid

state reaction (ceramic method) is a mature technique. In addition, it does not require a solvent to prepare spinel ferrites which can avoid any pollution from the solvent (Thakur, et al., 2015). In the solid state reaction, the grinding of oxalates, carbonates, oxides and other metal compounds is involved. The mixture will then be heated at high temperature (≥1 000 °C). The materials will undergo pelletizing, grinding and sintering processes until its desired phase is attained (Thakur, et al., 2015).

2.5.1 Synthesis of Ni-Zn Ferrite by Solid State Reaction from Pure Reagents

A nickel zinc ferrite with the composition of $Ni_{0.5}Zn_{0.5}Fe_2O_4$ was prepared by the solid state reaction. It involved iron (III) oxide and nitrates of the corresponding metals. The process was conducted in a porcelain crucible. The mixture underwent calcination at a very high temperature (1 073 K) for 50 hours. After that, it was regrinded every 10 hours (Knyazev, et al., 2015). Figure 2.7 shows the hysteresis loops of the synthesised nickel zinc ferrite which was measured at the temperature of 3 K and 300 K.

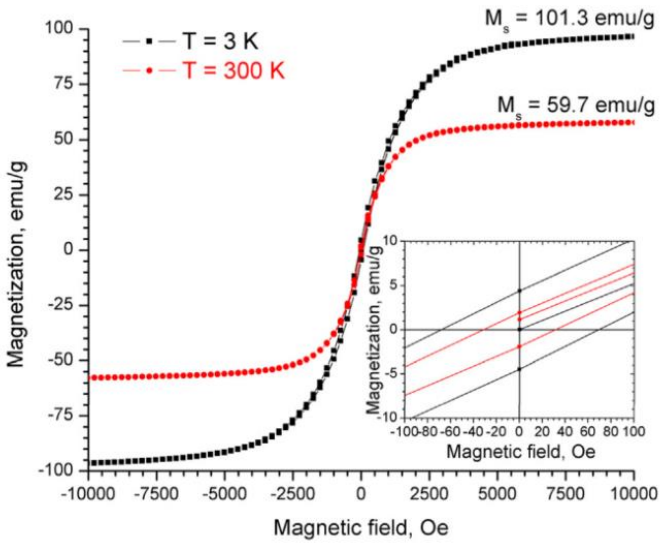

Figure 2.7: Hysteresis Loops of Synthesised Nickel Zinc Ferrite (3 K and 300 K Temperature) (Knyazev, et al., 2015).

Based on Figure 2.7, it shows that the synthesised $Ni_{0.5}Zn_{0.5}Fe_2O_4$ has the maximum saturation magnetization at 101.3 emu/g and the coercivity value of 68.9 Oe when measured at 3 K. However, when it was measured at 300 K, it

had the saturation magnetization of 59.7 emu/g and the lowest coercivity at 31.5 Oe (Knyazev, et al., 2015).

Another research was conducted on the synthesis of nickel zinc spinel ferrite ($(Ni_{0.5}Zn_{0.5})Fe_2O_4$) by the ceramic processing technique (solid state reaction). The mixture of zinc oxide, nickel (II) oxide, and iron (III) oxide underwent sintering process at a high temperature of 1 250 °C for 2 hours. Then, a sieve (average aperture size of 74 meters) was used to control the synthesised ferrite powders' particle size (Zhao, Lv and Shen, 2009). The X-ray diffraction pattern of the $(Ni_{0.5}Zn_{0.5})Fe_2O_4$ was shown in Figure 2.8.

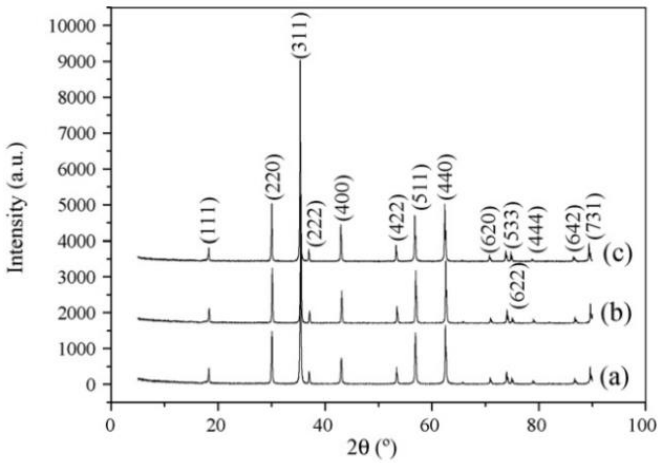

Figure 2.8: The X-ray Diffraction Pattern of Synthesised $(Ni_{0.5}Zn_{0.5})Fe_2O_4$, $(Ni_{0.4}Cu_{0.2}Zn_{0.4})Fe_2O_4$, and $(Ni_{0.4}Co_{0.2}Zn_{0.4})Fe_2O_4$ Ferrites Represented by (a), (b) and (c) respectively (Zhao, Lv and Shen, 2009).

Figure 2.9 shows that the recorded coercivity (Hc) and saturation magnetization (Ms) of the $(Ni_{0.5}Zn_{0.5})Fe_2O_4$ is 24 Oe and 83.48 emu/g respectively.

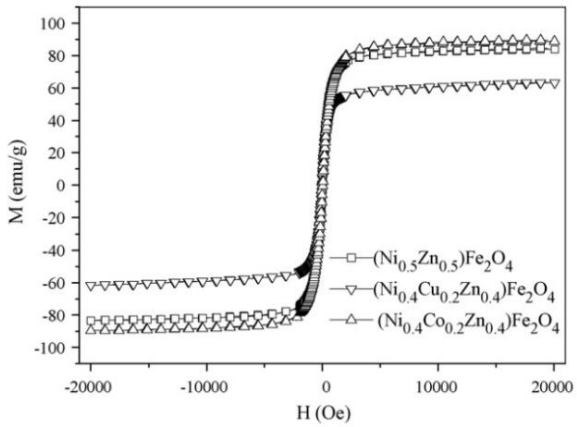

Fig. 3. Hysteresis loops of $(Ni_{0.5}Zn_{0.5})Fe_2O_4$, $(Ni_{0.4}Cu_{0.2}Zn_{0.4})Fe_2O_4$ and $(Ni_{0.4}Co_{0.2}Zn_{0.4})Fe_2O_4$ spinel ferrites.

Figure 2.9: The Hysteresis Loop of Synthesised $(Ni_{0.5}Zn_{0.5})Fe_2O_4$ Ferrite, $(Ni_{0.4}Cu_{0.2}Zn_{0.4})Fe_2O_4$ Ferrite and $(Ni_{0.4}Co_{0.2}Zn_{0.4})Fe_2O_4$ Ferrite (Zhao, Lv and Shen, 2009).

2.5.2 Synthesis of Ni-Zn Ferrite by Solid State Reaction from EAF Dust

There were a few researches conducted on the synthesis of the spinel ferrites from the steel dust waste. For example, the zinc bearing electric arc furnace dust, ZEAFD with the addition of nickel (II) hydroxide, $Ni(OH)_2$ were utilised to prepare the nickel zinc spinel ferrite, $(Ni,Zn)Fe_2O_4$. The solid state reaction technique was utilised to prepare the ferrite sample. Also, different mass ratios, $R_{ZE/N}$ (zinc bearing electric arc furnace dust to nickel (II) hydroxide) such as 2:0.3, 2:0.5, 2:0.7 and 2:0.9 were used. The dust was grinded with nickel (II) hydroxide. The sample was then heated at 800, 900 or 1 000 °C for 2 hours in a muffle furnace. The heating rate of 5 °C/min was used for the heating process. After the calcination process, the samples were cooled to room temperature (Wang, et al., 2020).

Figure 2.10 and Figure 2.11 show the X-ray diffraction pattern of the calcined nickel zinc spinel ferrite sample and washed nickel zinc spinel ferrite sample respectively.

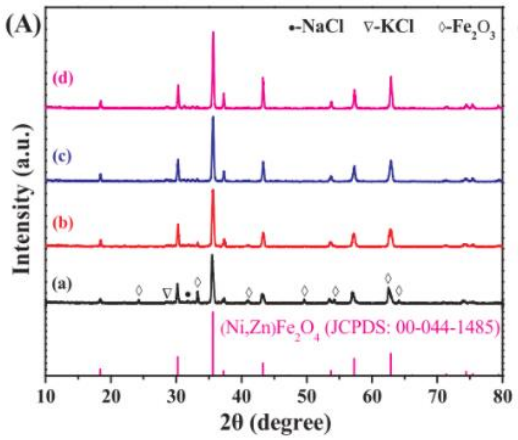

Figure 2.10: X-ray Diffraction Pattern of the Calcined Nickel Zinc Spinel Ferrite (Wang, et al., 2020).

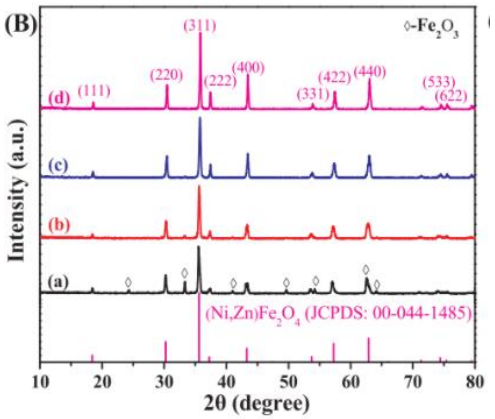

Figure 2.11: X-ray Diffraction Pattern of the Washed Nickel Zinc Spinel Ferrite (Wang, et al., 2020).

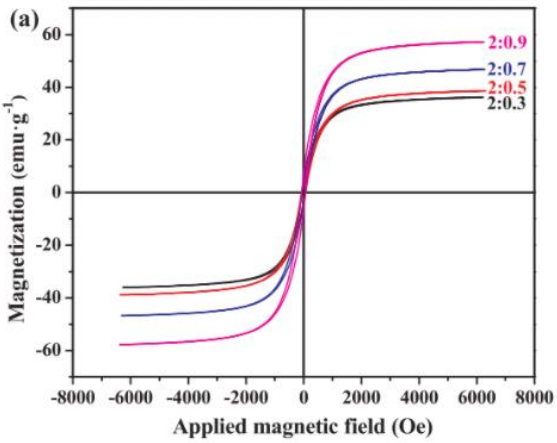

Figure 2.12: The Hysteresis Loop of Washed Nickel Zinc Spinel Ferrite (Wang, et al., 2020).

Based on the hysteresis loop as shown in Figure 2.12, the highest saturation magnetization recorded was 57.3 emu/g while its coercivity was 58.8 Oe when the mass ratio, $R_{ZE/N}$ was 2:0.9 and the calcination temperature was 1000 °C. In addition, the implemented toxicity assessment specified that the synthesised nickel zinc spinel ferrite was not toxic (Wang, et al., 2020).

The second example from a research which also utilised the zinc-containing electric arc furnace dust (EAFD) as a raw material to prepare a metal doped nickel zinc ferrite. Figure 2.13 shows the procedure of the solid state reaction to prepare the nickel zinc ferrite (Wang, et al., 2017).

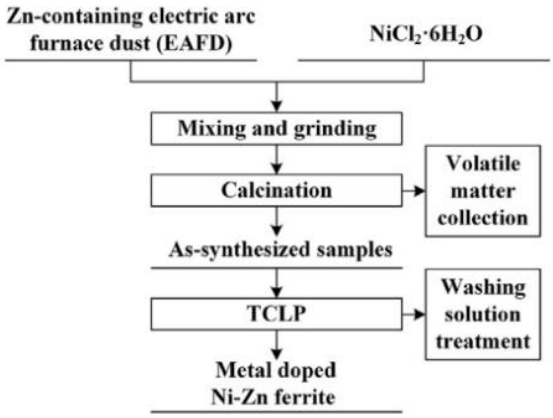

Figure 2.13: Procedure of Solid State Reaction for Metal Doped Nickel Zinc Ferrite (Wang, et al., 2017).

Firstly, the dust and nickel (II) chloride were mixed and grinded as shown in Figure 2.13. In the heating or calcination process, the mixture was heated to 1000 °C for 2 hours. Then, the synthesised sample underwent the toxicity characteristic leaching procedure, TCLP as shown in Figure 2.13. Finally, the washed nickel zinc ferrite sample was dried at a high temperature of 105 °C for 24 hours (Wang, et al., 2017).

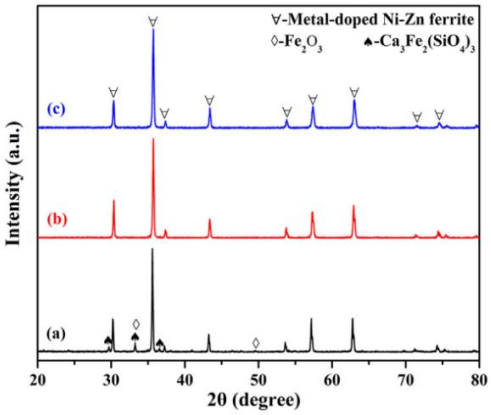

Figure 2.14: The X-ray Diffraction Pattern of the Synthesised Sample with Varying $R_{ZE/N}$ (a) 2:0.8, b) 2:1.2, c) 2:1.6) (Wang, et al., 2017).

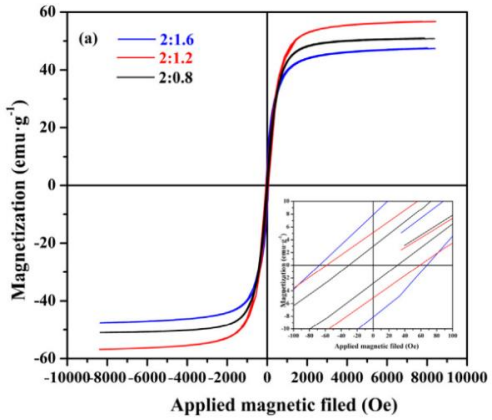

Figure 2.15: Hysteresis Loop of Synthesised Nickel Zinc Spinel Ferrite (Wang, et al., 2017).

Based on the hysteresis loop as shown in Figure 2.15, the highest saturation magnetization recorded was 56.8 emu/g while its coercivity was 58.5 Oe when the mass ratio, $R_{ZE/N}$ (zinc-containing electric arc furnace dust to nickel (II) chloride) was 2:1.2. In addition, the conducted toxicity evaluation specified that the synthesised nickel zinc spinel ferrite was not toxic (Wang, et al., 2017).

2.6 Synthesis of Metal(s)-Doped Zinc Ferrite

The magnesium-doped zinc ferrite was synthesized by the hydrothermal approach. Iron(III) nitrate nonahydrate ($Fe(NO_3)_3 \cdot 9H_2O$), magnesium nitrate hexahydrate ($Mg(NO_3)_2 \cdot 6H_2O$), and zinc nitrate hexahydrate ($Zn(NO_3)_2 \cdot 6H_2O$) were utilised to synthesize the Mg-Zn ferrite. The formula of the synthesized magnesium-doped zinc ferrite was $Mg_{1-x}Zn_xFe_2O_4$, where x (zinc content) was

0.4, 0.5, 0.6, and 0.7. There was around 0.75 g of yield of the synthesized sample per batch. The effect of the zinc content on the magnetic performance of the magnesium zinc ferrite was studied. The results indicated that the synthesized magnesium-doped zinc ferrite had the soft magnetic properties. Besides, when the zinc content increased, the saturation magnetization, Ms would rise. The synthesized samples had the coercivity, Hc value smaller than 35 Oe. The list of magnetic performance for different amount of zinc content of the synthesized sample were shown in Table 2.2. The highest saturation magnetization recorded was 44.5 emu/g when the zinc content, x was 0.4 (Tsay, Chiu and Tseng, 2019).

Table 2.2: The Magnetic Properties (Ms and Hc) of the Synthesized $Mg_{1-x}Zn_xFe_2O_4$ (Tsay, Chiu and Tseng, 2019).

Zinc content (x)	Ms (emu/g)	Hc (Oe)
0.4	44.5	32.7
0.5	38.6	32.5
0.6	32.6	34.2
0.7	22.6	32.4

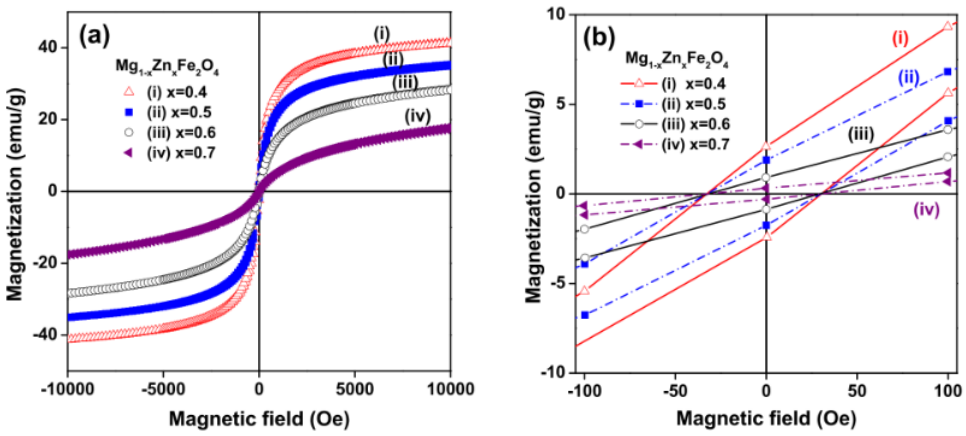

Figure 2.16: (a) Comparison of the Hysteresis Loops of the Synthesized $Mg_{1-x}Zn_xFe_2O_4$ with Different Zinc Content, and (b) Mganified View of (a) from -100 Oe to 100 Oe (Tsay, Chiu and Tseng, 2019).

Another study was conducted to examine the influence of cobalt ions (Co^{2+}) content on the magnetic performance of the synthesized cobalt-doped zinc ferrite. The formula of the synthesized cobalt-doped zinc ferrite was Zn_{1-}

$_xCo_xFe_2O_4$, where x (cobalt content) is 0.0, 0.1, 0.2, 0.3, 0.4, and 0.5. Iron(III) nitrate nonahydrate ($Fe(NO_3)_3 \cdot 9H_2O$), cobalt(II) nitrate hexahydrate ($Co(NO_3)_2 \cdot 6H_2O$), zinc nitrate hexahydrate ($Zn(NO_3)_2 \cdot 6H_2O$) and sodium hydroxide (NaOH) were utilised as the precipitant for the synthesis of the cobalt-doped zinc ferrite. The co-precipitation technique was used to synthesize the $Zn_{1-x}Co_xFe_2O_4$ (Tatarchuk, et al., 2018). Based on Table 2.3, when the cobalt content (x) increases, the saturation magnetization, Ms and coercivity, Hc of the synthesized cobalt-doped zinc ferrite rise.

Table 2.3: The Magnetic Properties (Ms and Hc) of the Synthesized $Zn_{1-x}Co_xFe_2O_4$ (Tatarchuk, et al., 2018).

Cobalt content (x)	Ms (emu/g)	Hc (Oe)
0	2.6	0
0.1	5.7	5.03
0.2	8.7	20.1
0.3	24.0	24.3
0.4	47.0	27.7
0.5	82.0	75.4

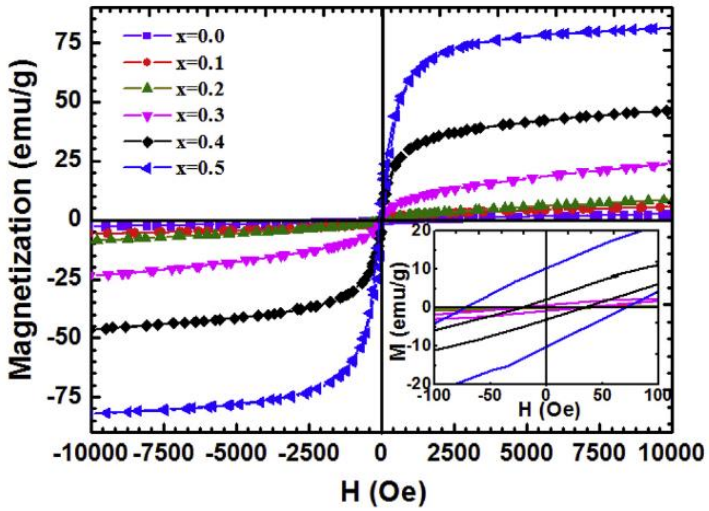

Figure 2.17: The Hysteresis Loops of Synthesised Cobalt-doped Zinc Ferrite with Different Cobalt Content (x) (Tatarchuk, et al., 2018).

Besides, study on the several doping of metal ions into the spinel ferrite was conducted. The manganese doped cobalt zinc ferrite was synthesized by sol-gel auto combustion method. The chemical reagents used for the synthesis of the manganese doped cobalt zinc ferrite include zinc (II) nitrate hexahydrate ($Zn(NO_3)_2 \cdot 6H_2O$), cobalt (II) nitrate hexahydrate ($Co(NO_3)_2 \cdot 6H_2O$), ferric (III) nitrate nonahydrate ($Fe(NO_3)_3 \cdot 9H_2O$), ammonium hydroxide and citric acid anhydrous. The effect of the manganese content (x) on the magnetic performance of the synthesized of $Mn_xCo_{0.5-x}Zn_{0.5}Fe_2O_4$, where x is 0.0, 0.1, 0.2, 0.3, and 0.4 was studied. Based on Table 2.4, it shows that when there was no manganese (x = 0) in the synthesized sample, the recorded saturation magnetization, Ms (77.31 emu/g) and coercivity, Hc (34.63 Oe) is higher than the manganese doped cobalt zinc ferrite samples. The highest saturation magnetization and coercivity obtained for the manganese doped cobalt zinc ferrite sample was when the manganese content (x) was 0.2. $Mn_{0.2}Co_{0.3}Zn_{0.5}Fe_2O_4$ had the highest saturation magnetization and coercivity at 75.30 emu/g and 31.31 Oe respectively (Mahajan, Godara and Srivastava, 2022).

Table 2.4: The Magnetic Properties (Ms and Hc) of the Synthesized $Mn_xCo_{0.5-x}Zn_{0.5}Fe_2O_4$ (Mahajan, Godara and Srivastava, 2022).

Manganese content (x)	Ms (emu/g)	Hc (Oe)
0	77.31	34.63
0.1	63.03	28.80
0.2	75.30	31.31
0.3	54.80	18.07
0.4	56.28	16.01

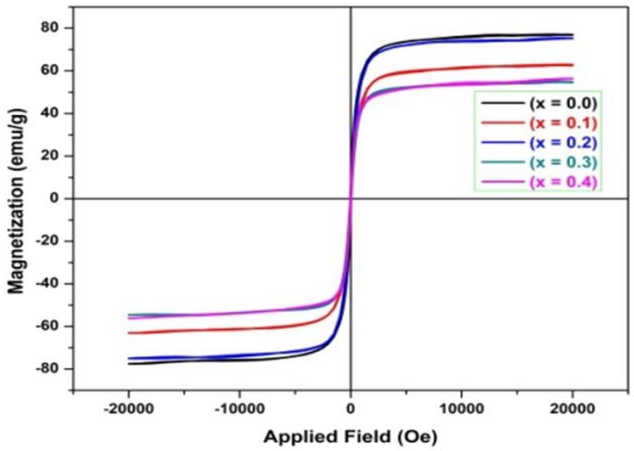

Figure 2.18: The Hysteresis Loops of Synthesised Manganese Doped Cobalt Zinc Ferrite with Different Manganese Content (x) (Mahajan, Godara and Srivastava, 2022).

2.7 Summary

The electric-arc furnace dust (EAFD) is a type of steel dust waste which is commonly generated during the production of steel. The generation of the amount of the electric-arc furnace dust will continue to increase due to the rising production of steel. The presence of cadmium, lead, and chromium make the dust hazardous to human health and environment. However, the valuable metal elements from the dust can be recovered with different types of proven techniques such as pyrometallurgical and hydrometallurgical methods.

The nickel zinc ferrite which is a mixed spinel ferrite contains attractive soft magnetic properties such as low coercivity and high magnetic saturation. In this project, it will be developed for magnetic sensors. It is suitable for the high frequency applications which are above 1 MHz.

The nickel zinc ferrite can be prepared by solid state reaction with pure reagents or EAF dust. The solid state reaction (ceramic technique) is a mature technique. Its starting materials are cheap and widely available in the industry. The prepared nickel zinc ferrite with pure reagents has the saturation magnetization value around 59.7 to 83.48 emu/g and the coercivity value around 24 to 31.5 Oe. However, the prepared nickel zinc ferrite from the EAF dust has the saturation magnetization value around 57 emu/g and the coercivity value around 58 Oe. Therefore, the prepared nickel doped zinc ferrite from the EAF dust or steel dust in this project should exhibit high saturation magnetization,

Ms (approximately at or higher than 57 emu/g) and low coercivity, Hc (approximately at or lower than 58 Oe) (Kumbhar, et al., 2014).

The list of comparison of the magnetic performance or magnetic properties among the nickel-doped zinc ferrite and other metal(s) doped zinc ferrite is shown in Table 2.5 below. The magnetic performance such as saturation magnetization, Ms and coercivity, Hc were compared.

Table 2.5: The List of Comparison for the Magnetic Performance of Spinel Ferrites.

Spinel Ferrite (with Materials Used)	Conditions	Ms (emu/g)	Hc (Oe)	Citation
Synthesis of Ni-Zn Ferrite by Solid State Reaction from Pure Reagents				
$Ni_{0.5}Zn_{0.5}Fe_2O_4$ (Iron (III) oxide and nickel nitrates)	• Calcination temperature was 1073 K for 50 hours. • Measurement temperature was 3 K.	101.30	68.90	(Knyazev, et al., 2015)
	• Calcination temperature was 1073 K for 50 hours. • Measurement temperature was 300 K.	59.70	31.50	(Knyazev, et al., 2015)
$(Ni_{0.5}Zn_{0.5})Fe_2O_4$ (Zinc oxide, nickel (II) oxide, and iron (III) oxide)	The sintering temperature was 1250 °C for 2 hours.	83.48	24.00	(Zhao, Lv and Shen, 2009)
Synthesis of Ni-Zn Ferrite by Solid State Reaction from EAF Dust				
$(Ni,Zn)Fe_2O_4$	The calcination temperature was	57.30	58.80	(Wang, et al., 2020)

(ZEAFD and nickel (II) hydroxide)	1000 °C (2 hours) and the mass ratio, $R_{ZE/N}$ was 2:0.9.			
$(Ni,Zn)Fe_2O_4$ (ZEAFD and nickel(II) chloride hexahydrate)	The calcination temperature was 1000 °C (2 hours) and the $R_{ZE/N}$ was 2:1.2.	56.80	58.50	(Wang, et al., 2017)
Synthesis of Metal(s)-Doped Zinc Ferrite				
$Mg_{1-x}Zn_xFe_2O_4$ (Iron(III) nitrate nonahydrate, magnesium nitrate hexahydrate, and zinc nitrate hexahydrate)	It was synthesized with the hydrothermal approach and the zinc content, x was 0.4.	44.50	32.70	(Tsay, Chiu and Tseng, 2019)
$Zn_{1-x}Co_xFe_2O_4$ (Iron(III) nitrate nonahydrate, cobalt(II) nitrate hexahydrate, zinc nitrate hexahydrate and sodium hydroxide)	It was synthesized with co-precipitation method and the cobalt content, x was 0.5.	82.0	75.4	(Tatarchuk, et al., 2018)
$Mn_xCo_{0.5-x}Zn_{0.5}Fe_2O_4$ (Zinc (II) nitrate hexahydrate, cobalt (II) nitrate hexahydrate, ferric (III) nitrate nonahydrate,	It was synthesized with sol-gel auto combustion method and the manganese content, x was 0.	77.31	34.63	(Mahajan, Godara and Srivastava, 2022)
	It was synthesized with sol-gel auto combustion method and the	75.30	31.31	(Mahajan, Godara and

ammonium hydroxide and citric acid anhydrous)	manganese content, x was 0.2.			Srivastava, 2022)

CHAPTER 3

METHODOLOGY AND WORK PLAN

3.1 Materials and Chemicals

The steel dust, electric-arc furnace dust (EAFD) which was given by industry was used in this project. The hydrochloric acid, HCl solution (37% w/w) was diluted with distilled water. The molarity of the diluted HCl solution was 0.5 mol/L and its volume was 200 mL. The purpose of the diluted HCL solution was to treat the EAFD. The nickel(II) chloride hexahydrate ($NiCl_2.6H_2O$) was selected to mix with the treated EAFD to synthesize the nickel zinc ferrite. Table 3.1 shows the list of chemical reagents utilised in this project.

Table 3.1: Chemical Reagents Used in This Project and Their Specifications.

Chemical Reagent	Purity (%)	Supplier	Usage
Hydrochloric acid, HCl	37	Sigma-Aldrich	It was for the treatment of EAFD.
Nickel(II) chloride hexahydrate, $NiCl_2.6H_2O$	98	Merck Millipore	It was mixed and ground with the treated EAFD to synthesize the nickel zinc ferrite samples.

3.2 Equipment and Instrument

Table 3.2 shows the list of the equipments for the synthesis of the nickel zinc ferrite samples. Table 3.3 shows the list of the instruments to characterise the synthesized nickel zinc ferrite samples.

Table 3.2: List of the Equipments.

Equipment	Purpose
Electromagnetic Stirrer	It was used to mix the diluted HCl (0.5 mol/L) solution and the EAFD during the treatment of the EAFD process.
Oven	It was used to dry the treated EAFD.
Annealing and Hardening Furnace	The mixture of the treated EAFD and Nickel(II) chloride hexahydrate ($NiCl_2.6H_2O$) was sintered in the furnace to form the nickel zinc ferrite compound.

Table 3.3: List of the Instruments.

Instrument	Instrument Model	Purpose
Scanning Electron Microscopy-Energy Dispersive X-ray (SEM-EDX)	Hitachi S-3400N Variable Pressure SEM	The generation of the surface morphology and the determination of the chemical composition of the EAFD and synthesized nickel zinc ferrite samples.
X-ray Diffractometer (XRD)	Shimadzu XRD-6000	The determination of the mineralogical phases of the EAFD and synthesized nickel zinc ferrite samples.
Fourier Transform Infrared Spectroscopy (FTIR)	Nicolet iS10	The indentification of the functional groups of the synthesized nickel zinc ferrite samples.
Vibrating Sample Magnetometer (VSM)	Lake Shore 7400 Series VSM system	The investigation of the magnetic properties of the synthesized nickel zinc ferrite samples.

3.3 Overall Research Methodology and Flow Diagram

Figure 3.1, and Figure 3.2 show the methodology plan for this project. Figure 3.3 shows the flow chart of the procedure to synthesize the nickel zinc ferrite samples if the practical experiment is allowed to conduct at the university. Based on Figure 3.1, the first plan (1) is to conduct practical experiment if the students are allowed to use the lab facilities in the university. The second plan (2) is to finish the project at hometown if the students are not allowed to go back to UTAR campus. In the project second plan (2), the data from the journals or research papers are collected to perform the data optimization with the Response Surface Methodology, RSM method. The Design Expert software will be used to simulate the data optimization. However, this second plan (2) was rejected as there were not enough data for the data optimization process. Hence, the first plan (1) was applied to complete this project. Besides, it was informed that the students are allowed to go back to the UTAR campus.

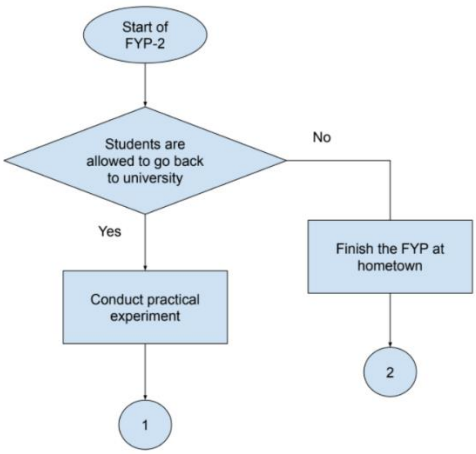

Figure 3.1: The Flow Chart of Methodology Plan Part I.

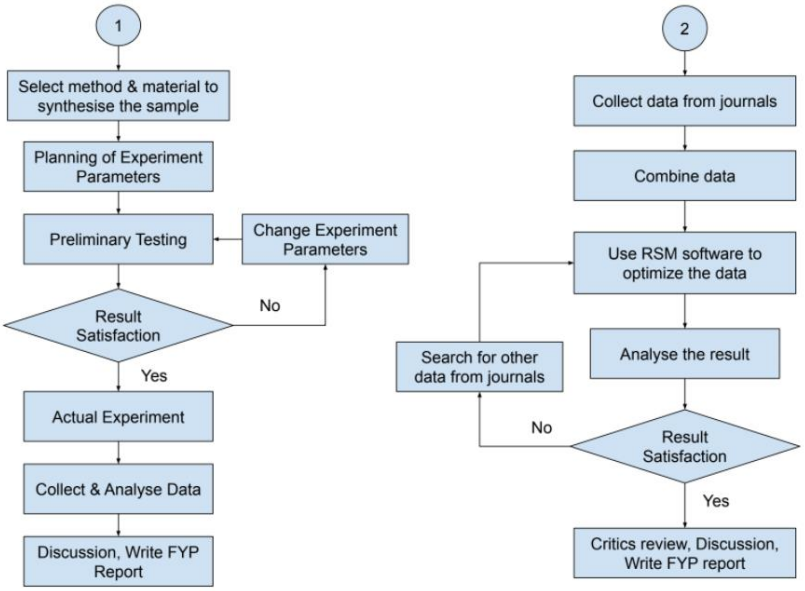

Figure 3.2: The Flow Chart of Methodology Plan Part II.

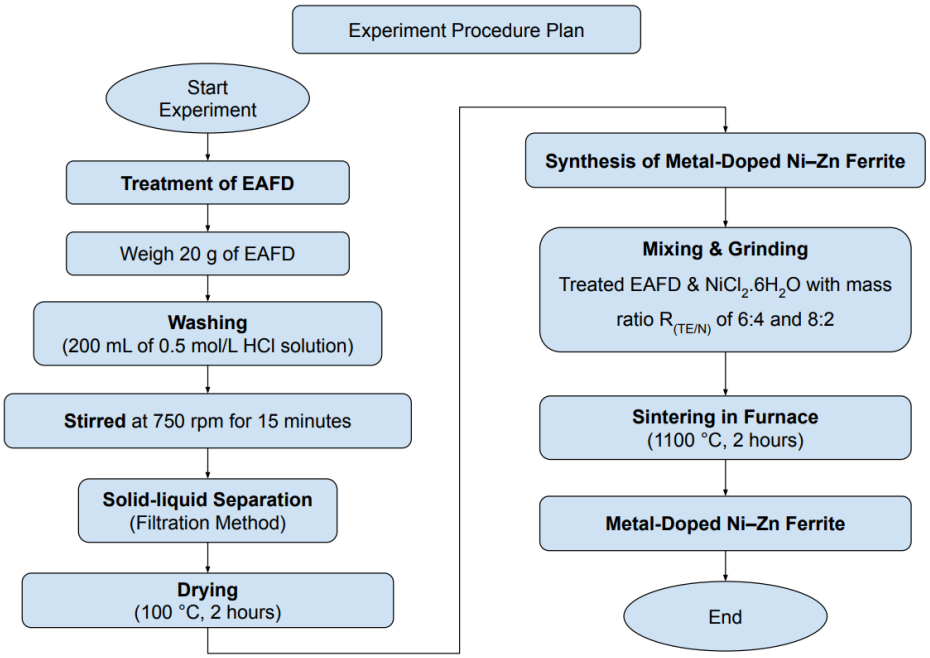

Figure 3.3: The Flow Chart of the Procedure to Synthesize the Nickel Zinc Ferrite Samples.

3.4 Experimental Procedures (Synthesis of the Nickel Zinc Ferrite Samples)

3.4.1 Electric-arc Furnace Dust (EAFD) Treatment

The hydrochloric acid, HCl solution (37% w/w) was diluted with the distilled water. To obtain 200 mL of the diluted HCl solution with the molarity of 0.5

mol/L, 8.2 mL of HCl solution (37% w/w) was mixed with 191.8 mL of distilled water. After that, 20 g of the EAFD was weighed with the analytical balance. The measured EAFD was then mixed with the diluted HCl solution in a beaker. An electromagnetic stirrer was used to stir the EAFD and diluted HCl solution mixture at 750 rpm (Scale of 5) for 15 minutes as shown in Figure 3.4. Then, solid-liquid separation was performed on the mixture by filtration as shown in Figure 3.5. The filtrate was collected in the erlenmeyer flask. The solids which accumulated on the filter paper was dried in the drying oven as shown in Figure 3.6 at 100 °C for 2 hours. The treated EAFD was obtained.

Figure 3.4: The Mixture of the EAFD with the Diluted HCl (0.5 mol/L) Solution in the Beaker Placed on the Electromagnetic Stirrer.

Figure 3.5: Solid Liquid Separation by Filtration.

Figure 3.6: Drying Oven Used in this Project.

3.4.2 Synthesis of the Nickel Zinc Ferrite Samples

The dried treated EAFD was mixed with the nickel(II) chloride hexahydrate, $NiCl_2.6H_2O$ with the mass ratio $R_{(TE/N)}$ of 6:4 and 8:2. $R_{(TE/N)}$ is the mass ratio of treated EAFD to $NiCl_2.6H_2O$. The treated EAFD and $NiCl_2.6H_2O$ were mixed and ground in the mortar adequately as shown in Figure 3.7. The mixtures were then placed into the alumina crucible, and they were sintered in the annealing and hardening furnace as shown in Figure 3.8. The sintering temperature was 1100 °C and the time taken of the sintering process was 2 hours. After that, the nickel zinc ferrite samples was synthesized as shown in Figure 3.9.

Figure 3.7: The Treated EAFD and NiCl2.6H2O were Mixed and Ground in the Mortar.

Figure 3.8: Annealing and Hardening Furnace (Nabertherm K4/13) Used in this Project.

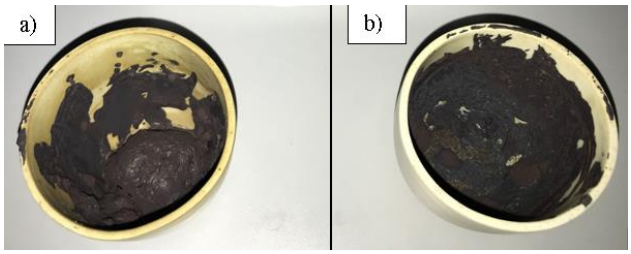

Figure 3.9: The Synthesized Nickel Zinc Ferrite Samples with the Mass Ratio R(TE/N) of (a) 6:4; and (b) 8:2.

3.5 Characterisation of the Synthesized Nickel Zinc Ferrite Samples

3.5.1 Scanning Electron Microscopy (SEM) with Energy Dispersive X-Ray (SEM-EDX)

The Scanning Electron Microscopy (SEM) was utilised to examine the the surface morphologies of the EAFD and the synthesized nickel zinc ferrite samples. During the specimen preparation, gloves were worn to prevent sample contamination. A carbon sticker was placed on each mounting pin tub. The sticky surface of the carbon sticker held the powder specimens. The specimens were ready for the SEM analysis. For the Energy Dispersive X-Ray (EDX), the chemical composition of the EAFD, treated EAFD and the synthesized nickel zinc ferrite samples were identified.

3.5.2 X-ray Diffraction (XRD)

The mineralogical phases of the EAFD and synthesized nickel zinc ferrite samples were generated by the X-ray Diffractometer (XRD). The specimen was placed on the XRD specimen holder as shown in Figure 3.10. The specimen on the holder was pressed by a glass plate as shown in Figure 3.10 to ensure that

the specimen would not fall off from the holder. During the measurement, the voltage and current of the X-ray Tube of the XRD was 40.0 kV and 30.0 (mA) respectively. Copper is the target material during the measurement. The scan range of the specimens was at the diffraction angle, 2θ ranging from 10.0 ° to 80.0 °. The scan speed and sampling pitch of the XRD was 2.0 ° per minute and 0.02 ° respectively.

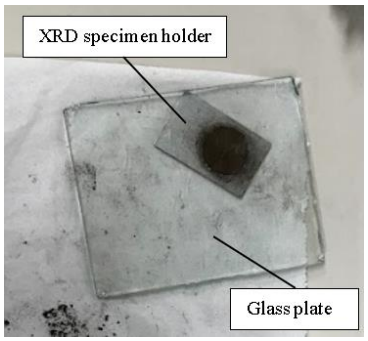

Figure 3.10: The Specimen Holder of XRD.

3.5.3 Fourier Transform Infrared Spectroscopy (FTIR Spectroscopy)

With the Fourier Transform Infrared (FTIR) spectroscope, the chemical or functional groups of the sample can be identified. Also, the XRD results can receive extra or complementary information from the FTIR's results (Berthomieu and Hienerwadel, 2009). The vibrational properties of the chemical bonds within the sample will be probed by the FTIR during the measurement. The chemical bonds of the sample will absorb the infrared radiation at their specific frequency which results in the detection of specific compounds in the sample (Berthomieu and Hienerwadel, 2009). The measured wavenumber of the FTIR in this project ranged from 4000 cm^{-1} to 400 cm^{-1}. The generated spectrum of each sample was then compared with the database's spectrum.

3.6 Parameter Study (Effect of Mass Ratio, $R_{(TE/N)}$ on the Magnetic Properties of Synthesized Ni-Zn Ferrite)

The effect of varying mass ratio, $R_{(TE/N)}$ on the magnetic properties of the synthesized nickel zinc ferrite were studied. $R_{(TE/N)}$ is the mass ratio of the

treated EAFD to nickel(II) chloride hexahydrate ($NiCl_2.6H_2O$). The treated EAFD and $NiCl_2.6H_2O$ were used to synthesize the nickel zinc ferrite. $R_{(TE/N)}$ of 6:4 and 8:2 were used in this project. The total mass of the treated EAFD and $NiCl_2.6H_2O$ mixture was 10 g for both samples. Varying $R_{(TE/N)}$ has impact on the magnetic properties of the synthesized spinel ferrite [A2]. In this project, the magnetic properties such as saturation magnetization (Ms), coercivity (Hci) and retentivity (Mr) of the synthesized nickel zinc ferrite were investigated and compared.

3.7 Vibrating Sample Magnetometer (VSM) Lake Shore 7400 Series

The magnetic properties of the synthesized nickel zinc ferrite samples were measured by the Vibrating Sample Magnetometer (VSM). The VSM lab facility service was provided by the Nanotechnology & Catalysis Research Centre (NANOCAT) which is located at the Institute for Advanced Studies from the University of Malaya. The maximum field used in the measurement was 8000 Gauss (G). The saturation magnetization (Ms), coercivity (Hci), and retentivity (Mr) of the synthesized nickel zinc ferrite samples were obtained from the VSM measurement.

Figure 3.11: The Vibrating Sample Magnetometer (VSM) by NANOCAT.

CHAPTER 4

RESULTS AND DISCUSSIONS

4.1 Characterisation of the Synthesized Nickel Zinc Ferrite Samples

4.1.1 Scanning Electron Microscopy (SEM) with Energy Dispersive X-Ray (SEM-EDX)

The SEM was utlized to inspect the surface morphologies of the EAFD and the synthesized nickel zinc ferrite samples under different mass ratio $R_{(TE/N)}$. Figure 4.1 shows the SEM images of the EAFD and synthesized nickel zinc ferrite with the $R_{(TE/N)}$ of 6:4 and 8:2 at 15000x Magnification. Figure 4.2 shows the SEM images of the EAFD and synthesized nickel zinc ferrite with the $R_{(TE/N)}$ of 6:4 and 8:2 at 6000x Magnification. Both synthesized nickel zinc ferrite samples with different $R_{(TE/N)}$ were sintered at 1100 °C for 2 hours.

Based on Figure 4.1 and Figure 4.2, it can be observed that all the particle size of the EAFD and synthesized nickel zinc ferrite with the $R_{(TE/N)}$ of 6:4 and 8:2 are non-uniform. The EAFD forms agglomerates of spherical particles as shown in Figure 4.1 (a) and Figure 4.2 (a). For the synthesized nickel zinc ferrite with the $R_{(TE/N)}$ of 6:4, it can be seen that it is composed of octahedral and cubic shape particle with smooth surface as shown in Figure 4.1 (b) and Figure 4.2 (b). For the synthesized nickel zinc ferrite with the $R_{(TE/N)}$ of 8:2, it is composed of irregular shape particles as shown in Figure 4.1 (c) and Figure 4.2 (c), and its particles size are larger than that of the $R_{(TE/N)}$ of 6:4. This can indicate that when the nickel (Ni) content within the nickel zinc ferrite compound increases, the grain size of the nickel zinc ferrite compound decreases (Kumbhar, et al., 2014).

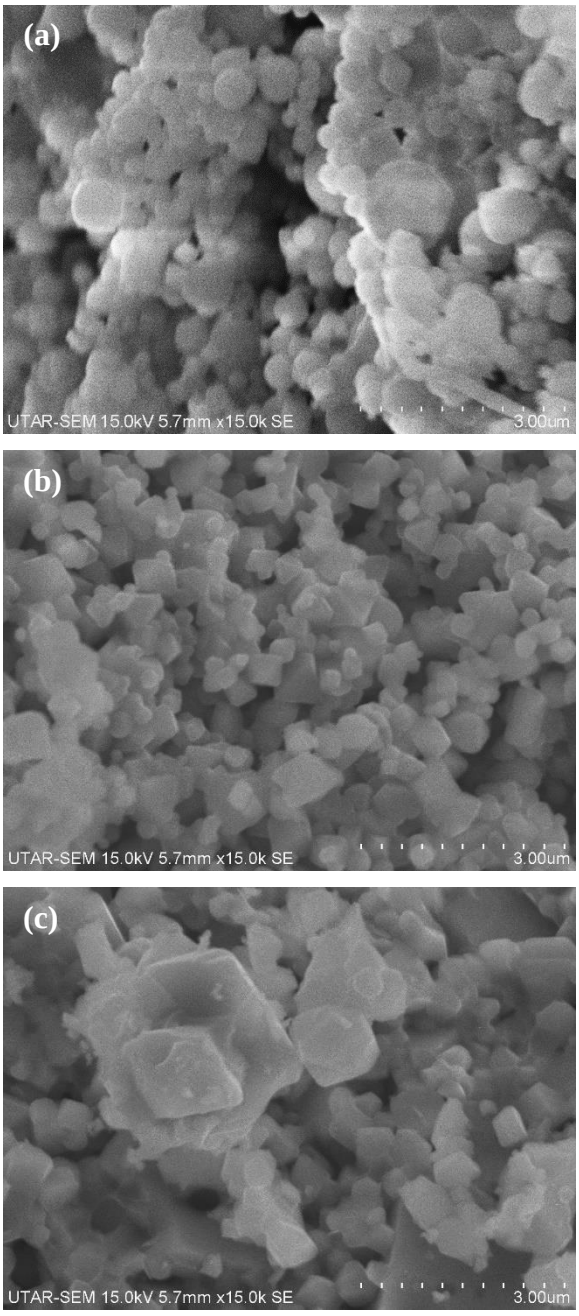

Figure 4.1: SEM Images of (a) EAFD, and Synthesized Ni-Zn Ferrite with the Mass Ratio, $R_{(TE/N)}$ of (b) 6:4; and (c) 8:2 at 15000x Magnification.

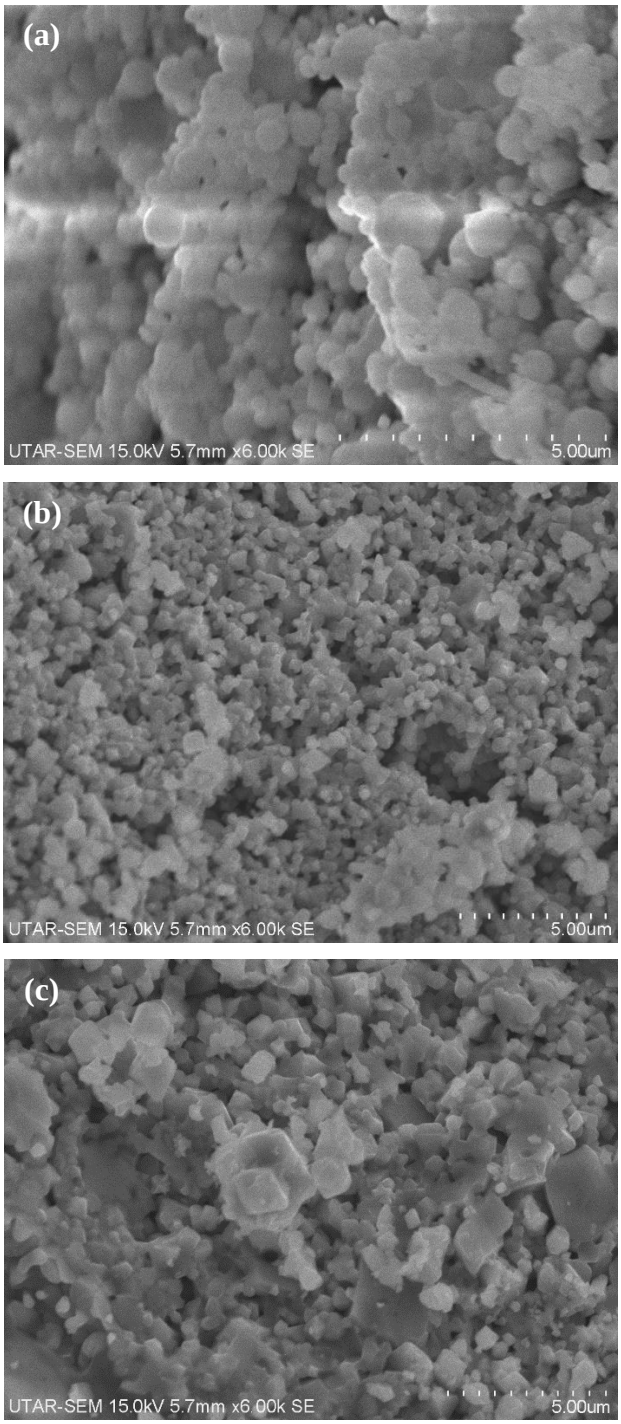

Figure 4.2: SEM Images of (a) EAFD, and Synthesized Ni-Zn Ferrite with the Mass Ratio, $R_{(TE/N)}$ of (b) 6:4; and (c) 8:2 at 6000x Magnification.

The weight percentage (Wt %) chemical composition of the EAFD, treated EAFD and synthesized nickel zinc ferrite samples were idendified by the EDX as shown in Table 4.1, Table 4.2, Table 4.3, and Table 4.4. Besides, the EDX spectrum of the EAFD, treated EAFD and synthesized nickel zinc ferrite samples were generated by the EDX as shown in Figure 4.3, Figure 4.4, Figure

4.5, and Figure 4.6. Based on Table 4.1 and Table 4.2, the weight percentage of the zinc (Zn) and iron (Fe) elements in the treated EAFD are lower than that of the EAFD. This indicates that the some of the Zn and Fe contents were removed by the diluted HCl solution during the treatment of the EAFD. The weight percentage of the nickel (Ni) element in the synthesized sample with the $R_{(TE/N)}$ of 6:4 (26.12 Wt %) is higher than that of the $R_{(TE/N)}$ of 8:2 (4.13 Wt %) as shown in Table 4.3 and Table 4.4. This is due to the higher amount of Ni element used in the synthesized sample with the $R_{(TE/N)}$ of 6:4 as compared to that of the $R_{(TE/N)}$ of 8:2 during the synthesis of the sample. Furthermore, the weight percentage of the Fe and Zn elements in the synthesized sample with the $R_{(TE/N)}$ of 8:2 are greater than that of the $R_{(TE/N)}$ of 6:4 as shown in Table 4.4 and Table 4.3. This is due to the higher amount of treated EAFD used in the synthesized sample with the $R_{(TE/N)}$ of 8:2 as compared to that of the $R_{(TE/N)}$ of 6:4 during the synthesis of the sample.

Table 4.1: Chemical Composition of EAFD.

Element	Weight Percentage (Wt%)
O	13.94
Pb	2.58
Cd	1.32
Ca	2.70
Cr	0.72
Fe	48.83
Zn	29.91

Table 4.2: Chemical Composition of Treated EAFD.

Element	Weight Percentage (Wt%)
O	19.47
Na	11.77
Mg	1.16
Al	0.68
Si	1.36
Cl	0.64
K	0.51
Ca	0.81
Cr	0.77
Mn	3.49
Fe	43.75
Zn	15.59

Table 4.3: Chemical Composition of Synthesized Ni-Zn Ferrite with the $R_{(TE/N)}$ of 6:4.

Element	Weight Percentage (Wt%)
O	13.30
Na	4.11
Mg	0.49
Al	0.19
Si	0.19
S	0.16
Cl	0.11
K	0.38
Ca	0.47
Cr	0.88
Mn	2.91
Fe	38.87
Ni	26.12
Zn	11.83

Table 4.4: Chemical Composition of Synthesized Ni-Zn Ferrite with the $R_{(TE/N)}$ of 8:2.

Element	Weight Percentage (Wt%)
O	16.56
Na	6.88
Mg	0.48
Al	0.28
Si	1.28
S	0.36
Cl	0.28
K	0.51
Ca	0.63
Cr	0.89
Mn	3.80
Fe	48.41
Ni	4.13
Zn	15.52

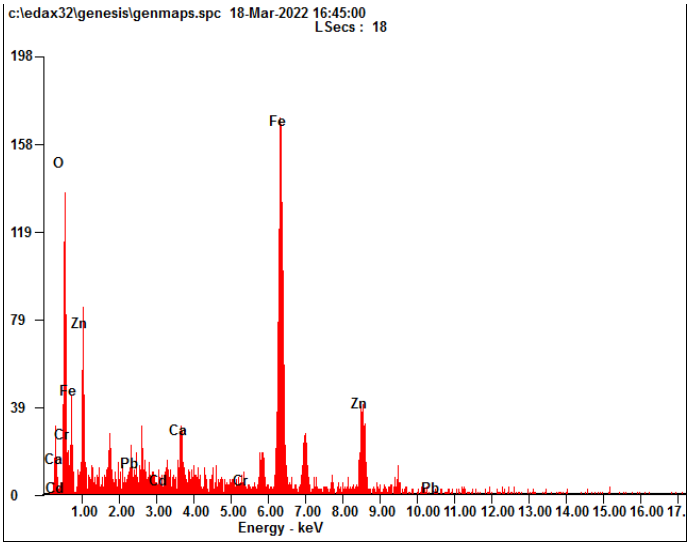

Figure 4.3: EDX Spectrum of EAFD.

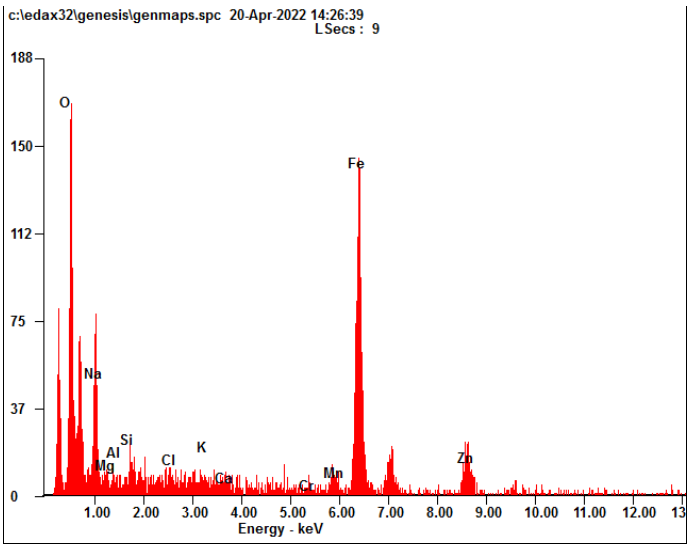

Figure 4.4: EDX Spectrum of Treated EAFD.

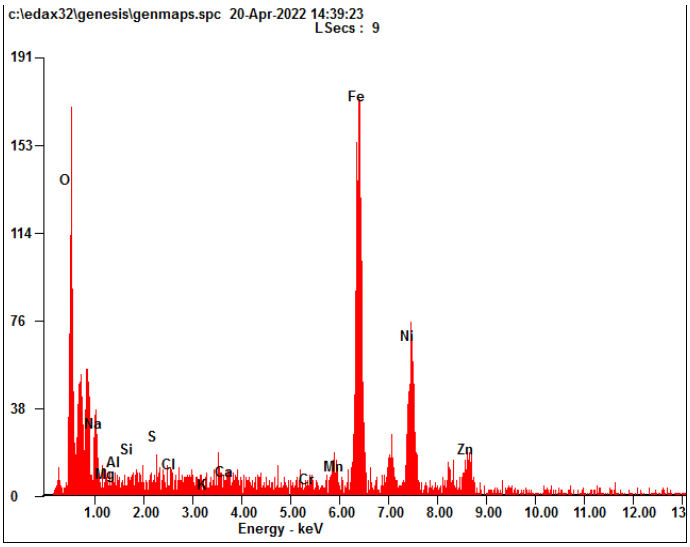

Figure 4.5: EDX Spectrum of Synthesized Ni-Zn Ferrite with the $R_{(TE/N)}$ of 6:4.

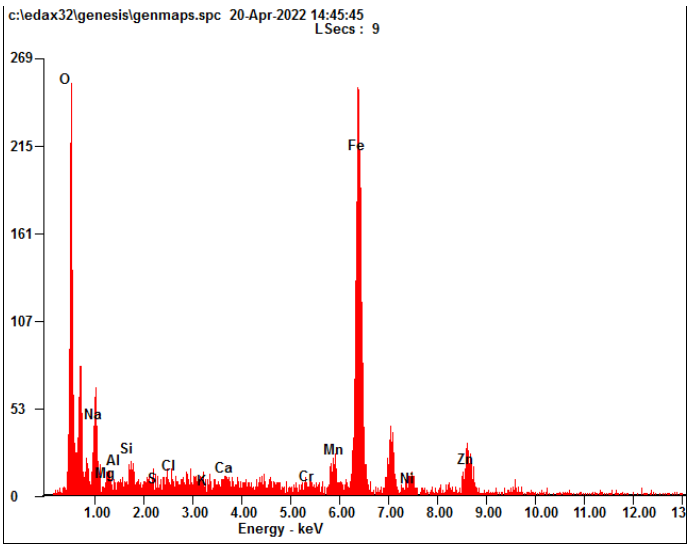

Figure 4.6: EDX Spectrum of Synthesized Ni-Zn Ferrite with the $R_{(TE/N)}$ of 8:2.

4.1.2 X-ray Diffraction (XRD)

The XRD was used to evaluate the mineralogical phases of the EAFD and synthesized nickel zinc ferrite samples. Figure 4.7 shows the XRD spectra of the EAFD. Figure 4.8 (A) shows the XRD spectra of the (a) EAFD, synthesized nickel zinc ferrite samples with $R_{(TE/N)}$ of (b) 8:2, and (c) 6:4. Figure 4.8 (B) shows the magnified view of XRD spectra of the (a) EAFD, synthesized nickel zinc ferrite samples with $R_{(TE/N)}$ of (b) 8:2, and (c) 6:4 from 35° to 36°.

Based on Figure 4.7, it is shown that the franklinite, $ZnFe_2O_4$ and magnetite, Fe_3O_4 are the major phases in the XRD spectra of the EAFD. Both

$ZnFe_2O_4$ and Fe_3O_4 are represented by the blue triangle symbol as shown in Figure 4.7. The calcium carbonate ($CaCO_3$), and potassium chloride (KCl) are the minor phases in the XRD spectra of the EAFD (Wang, et al., 2020).

Based on Figure 4.8 (b) and (c), the XRD spectra of the synthesized samples were compared to that of $Ni_{0.5}Zn_{0.5}Fe_2O_4$ (COD ID: 9009920). It is shown that the diffraction peaks of the synthesized nickel zinc ferrite samples with $R_{(TE/N)}$ of (b) 8:2, and (c) 6:4 match the that of the $Ni_{0.5}Zn_{0.5}Fe_2O_4$ (COD ID: 9009920). Hence, this indicates that pure nickel zinc ferrite was synthesized (Wang, et al., 2020). Besides, no iron(III) oxide (Fe_2O_3) was found within the XRD spectra of the synthesized nickel zinc ferrite samples. Sufficient mass of $NiCl_2 \cdot 6H_2O$ was used during the synthesis of the nickel zinc ferrite samples may result in the absence of Fe_2O_3 in the synthesized samples. When the there was sufficient of $NiCl_2 \cdot 6H_2O$ in the mixture, the amount of generated nickel(II) oxide (NiO) increased. The generated NiO would then react with the $ZnFe_2O_4$ and Fe_3O_4 within the treated EAFD. Subsequently, $Ni_{0.5}Zn_{0.5}Fe_2O_4$ was formed as shown in the chemical equation (1).

$$xNiO + yFe_3O_4 + \frac{y}{4}O_2 + zZnFe_2O_4 =$$

$$(Ni_xZn_z)Fe_{2x+2z}O_{4x+4z} + \frac{3y-2x}{2}Fe_2O_3 \quad (3y > 2x, \frac{Fe}{M} > 2.0) \qquad (1)$$

$$3CaCO_3 + 3SiO_2 + Fe_2O_3 = Ca_3Fe_2(SiO_4)_3 + 3CO_2 \qquad (2)$$

However, when the amount of $NiCl_2 \cdot 6H_2O$ was not sufficient, less NiO was generated to react with the $ZnFe_2O_4$ and Fe_3O_4. Hence, the resulted in the oxidation of the remaining Fe_3O_4 into the Fe_2O_3. Based on the chemical equation (2), the $Ca_3Fe_2(SiO_4)_3$ would be formed (Wang, et al., 2017). Therefore, there was no Fe_2O_3 generated during the synthesis of the samples in this project due to the amount of $NiCl_2 \cdot 6H_2O$ used was sufficient.

Furthermore, based on Figure 4.8 (B), it shows that the highest diffraction peak which is the (3 1 1) crystal plane shifts from 35.54° to 35.66° when the $R_{(TE/N)}$ changes from 8:2 to 6:4. The shift of the diffraction peak to high 2θ angle value may be due to the increasing amount of nickel (Ni) element within the synthesized nickel zinc ferrite compound. The ionic radius of nickel which is 0.069 nm is smaller than that of zinc (II) ion, Zn^{2+} (0.074 nm) (Wang,

et al., 2020). The synthesized sample with the $R_{(TE/N)}$ of 6:4 has more nickel than that of the $R_{(TE/N)}$ of 8:2. Therefore, the (311) diffraction peak of the $R_{(TE/N)}$ of 6:4 is located at higher 2θ angle value compared to that of the $R_{(TE/N)}$ of 8:2.

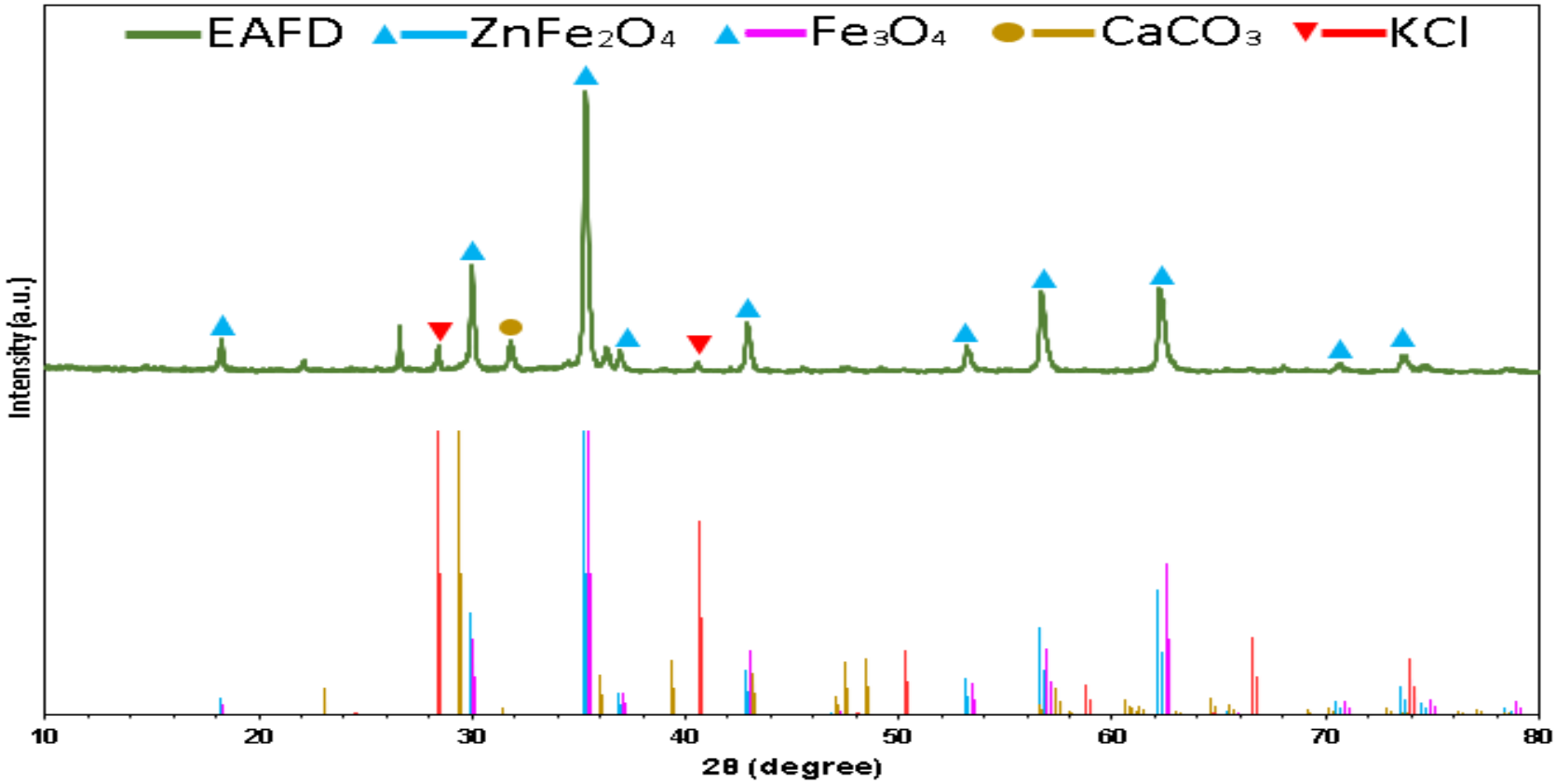

Figure 4.7: XRD spectra of the EAFD.

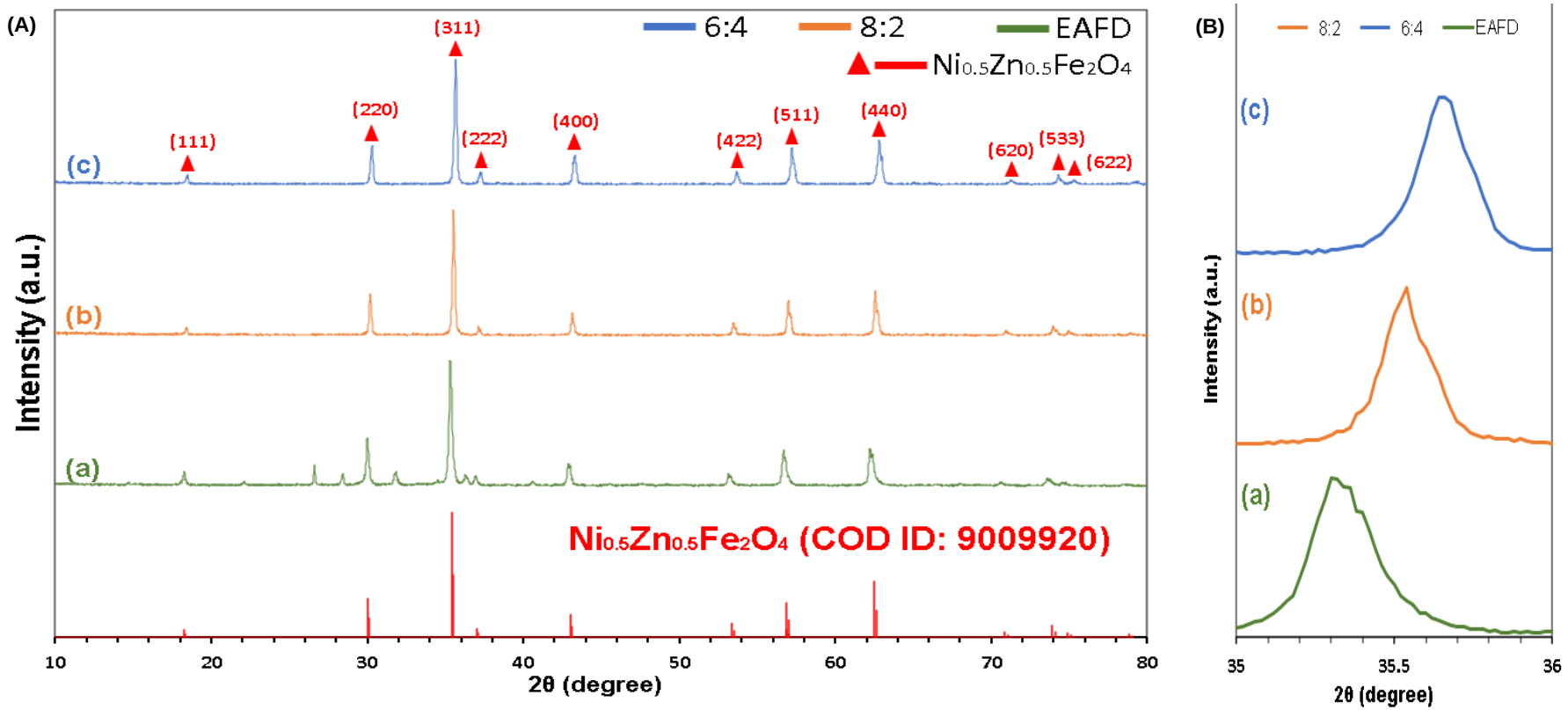

Figure 4.8: XRD spectra of (A) the Synthesized Ni-Zn Ferrite Samples and EAFD, and (B) the Magnified View of (A) from 35° to 36°, for Samples Synthesized with $R_{(TE/N)}$ of (b) 8:2, and (c) 6:4.

4.1.3 Fourier Transform Infrared Spectroscopy (FTIR Spectroscopy)

The FTIR was utilised to evaluate the functional groups within the synthesized nickel zinc ferrite samples. Figure 4.9 shows the FTIR Spectra of the Synthesized Nickel Zinc Ferrite with the $R_{(TE/N)}$ of 6:4. Figure 4.10 shows the FTIR Spectra of the Synthesized Nickel Zinc Ferrite with the $R_{(TE/N)}$ of 8:2.

Based on Figure 4.9 (a) and Figure 4.10 (a), 2 main metal oxygen absorption bands can be seen in the range of 400 to 600 cm^{-1} wavelength. The v_1 and v_2 represent the frequency bands around 400 cm^{-1} and 600 cm^{-1} respectively as shown in Figure 4.9 and Figure 4.10. Besides, the frequency bands around 400 cm^{-1} (v_1) and 600 cm^{-1} (v_2) represent the octahedral and tetrahedral metal oxygen vibration complexes respectively (Babu and Tatarchuk, 2018). The formation of single phase spinel ferrite which contains the octahedral and tetrahedral site of the sublattice was confirmed by these bands v_1 and v_2 (Kurian and Nair, 2016). For the synthesized sample with the $R_{(TE/N)}$ of 6:4, the v_1 and v_2 are located at 418 cm^{-1} and 568 cm^{-1} respectively as shown in Figure 4.9. For the synthesized sample with the $R_{(TE/N)}$ of 8:2, the v_1 and v_2 are located at 405 cm^{-1} and 576 cm^{-1} respectively as shown in Figure 4.10.

(a)

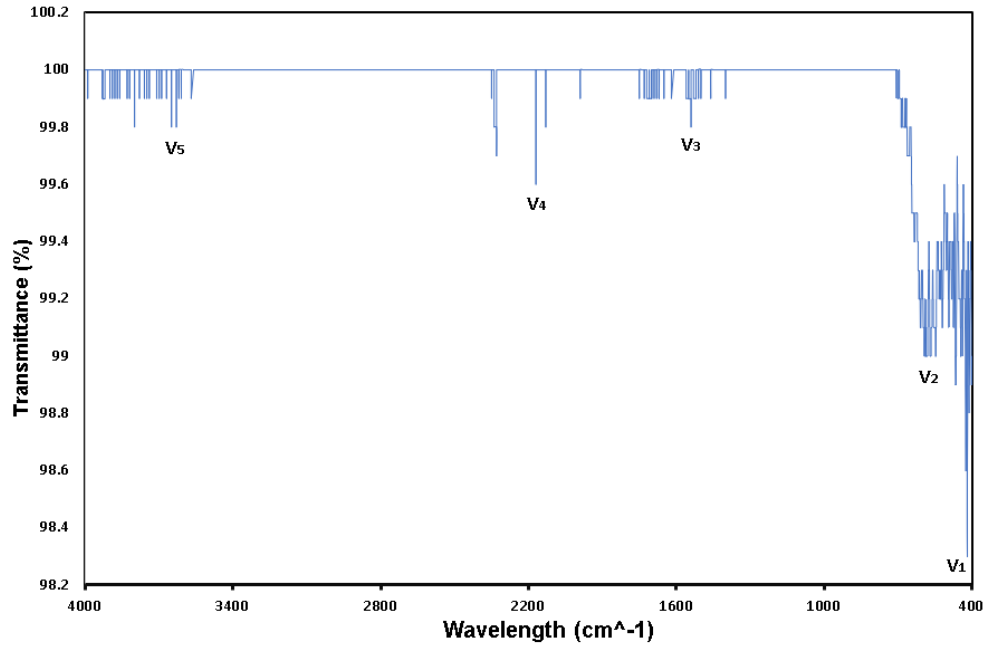

(b)

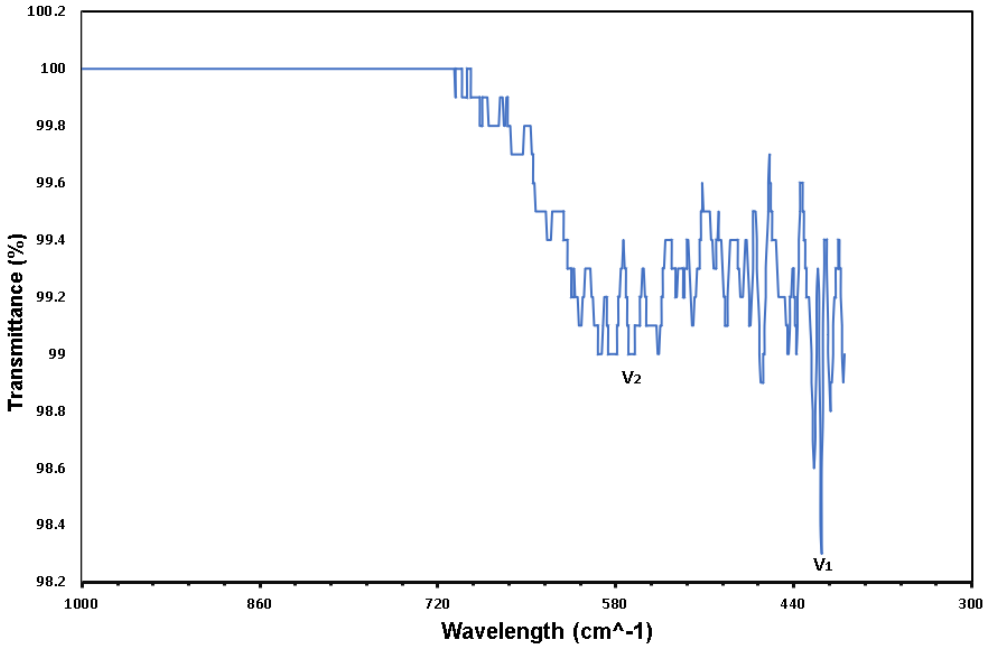

Figure 4.9: FTIR Spectra of the Synthesized Nickel Zinc Ferrite with the $R_{(TE/N)}$ of 6:4 (a) from 4000 cm^{-1} to 400 cm^{-1}, and (b) Magnified View of (a) from 1000 cm^{-1} to 400 cm^{-1}.

(a)

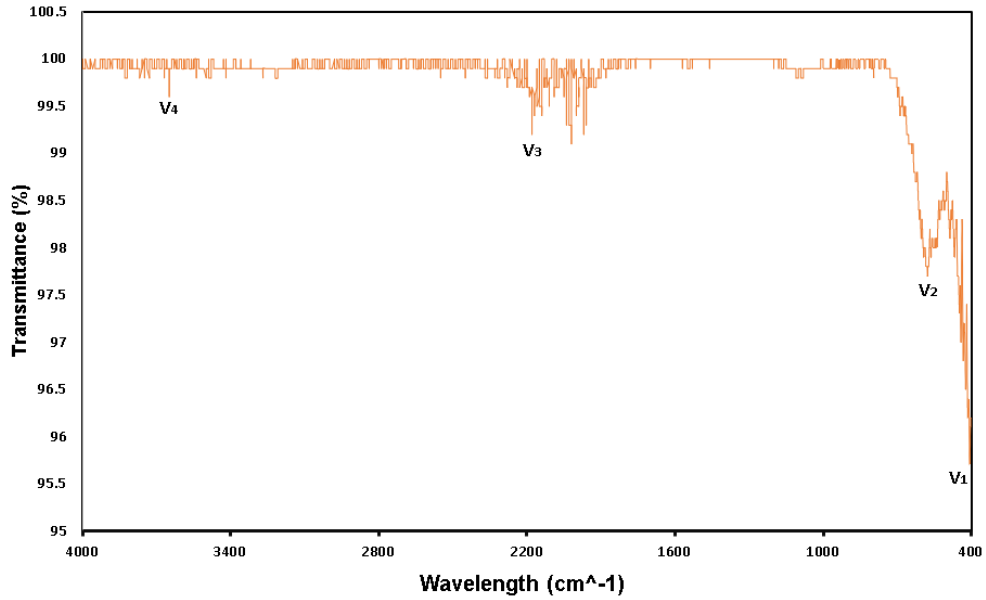

(b)

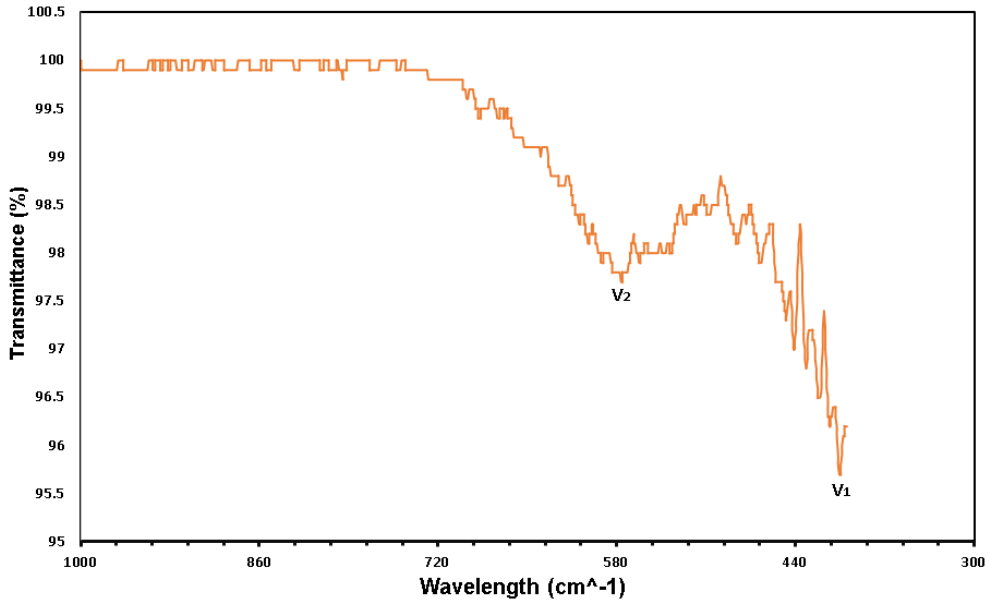

Figure 4.10: FTIR Spectra of the Synthesized Nickel Zinc Ferrite with the $R_{(TE/N)}$ of 8:2 (a) from 4000 cm^{-1} to 400 cm^{-1}, and (b) Magnified View of (a) from 1000 cm^{-1} to 400 cm^{-1}.

4.2 Parameter Study (Effect of Mass Ratio, $R_{(TE/N)}$ on the Magnetic Properties of Synthesized Ni-Zn Ferrite)

The Vibrating Sample Magnetometer (VSM) was used to identify the magnetic properties of the synthesized nickel zinc ferrite samples. The saturation magnetization (Ms), coercivity (Hci), and retentivity (Mr) of the samples were compared and analyzed. The coercivity is the measure of the external magnetic field required to demagnetize the magnetized material. The retentivity is defined as the ability of a magnetic material to maintain the magnetism without the presence of the magnetizing field.

Based on Figure 4.11, the blue hysteresis loop line represents the synthesized nickel zinc ferrite with the $R_{(TE/N)}$ of 6:4. The orange hysteresis loop line represents the synthesized nickel zinc ferrite with the $R_{(TE/N)}$ of 8:2 as shown in Figure 4.11. Figure 4.11 shows that the blue hysteresis loop is longer and wider than the orange hysteresis loop. Figure 4.12 indicates that the synthesized nickel zinc ferrite with the $R_{(TE/N)}$ of 6:4 has greater Ms, Hci and Mr than that of the $R_{(TE/N)}$ of 8:2. The synthesized nickel zinc ferrite with the $R_{(TE/N)}$ of 6:4 has Ms, Hci and Mr of 61.24 emu/g, 21.65 G, and 2.19 emu/g respectively. Then, The synthesized nickel zinc ferrite with the $R_{(TE/N)}$ of 8:2 has Ms, Hci and Mr of 47.37 emu/g, 6.43 G, and 0.58 emu/g respectively.

The saturation magnetization, Ms rises when the $R_{(TE/N)}$ changes from 8:2 to 6:4. This is due to the increasing quantity of nickel, Ni^{2+} element within the synthesized nickel zinc ferrite sample. The synthesized sample with the $R_{(TE/N)}$ of 6:4 has more nickel than that of the $R_{(TE/N)}$ of 8:2. In general, the difference between the octahedral B-sites' magnetic moment (M_B) and tetrahedral A-sites' magnetic moment (M_A) is the spinel ferrites' magnetic properties, M ($M=M_B-M_A$). When the value of M rises, the Ms will increase which results in higher magnetic performance of the spinel ferrite. The spinel ferrite has the general formula of AB_2O_4. The B-sites is more likely to occupied by the nickel (II) ions (Ni^{2+}) as compared to Al^{3+} and Mg^{2+} ions. Subsequently, when the concentration of Ni^{2+} rises, the Al^{3+} and Mg^{2+} ions will move from the B-sites to A-sites. This results in the rising of the value of M_B and Ms (Wang, et al., 2020).

The coercivity, Hci of the spinel ferrite is affected by the anisotropy throughout the magnetization's process and the spinel ferrite's grain size. The

synthesized sample with the $R_{(TE/N)}$ of 6:4 has more nickel content than that of the $R_{(TE/N)}$ of 8:2. Thus, the Hci value of the synthesized sample with the $R_{(TE/N)}$ of 6:4 (21.65 G) is higher than that of the $R_{(TE/N)}$ of 8:2 (6.43 G). This indicates that the anisotropy of the synthesized sample increased in the magnetic lattice (Wang, Guo and Zhang, 2017). Besides, the ferrite's grain size also influences the Hci value of the spinel ferrite. The growth of the grain size is due to the zinc element within the ferrite compound. Less energy is required for the magnetization under the influence of the domain wall movement as compared to that of the domain rotation (Džunuzović, et al., 2015). When the grain size increases due to the addition of zinc, the amount of domain walls rises. Consequently, the growing domain wall movement results in higher magnetization (Džunuzović, et al., 2015). In short, the sample has low Hci value when it has large grain size (Džunuzović, et al., 2015). The synthesized sample with the $R_{(TE/N)}$ of 8:2 could have larger grain size than that of the $R_{(TE/N)}$ of 6:4 as shown in Figure 4.1 (b) and (c). Thus, the Hci value of the synthesized sample with the $R_{(TE/N)}$ of 8:2 (6.43 G) is smaller than that of the $R_{(TE/N)}$ of 6:4 (21.65 G).

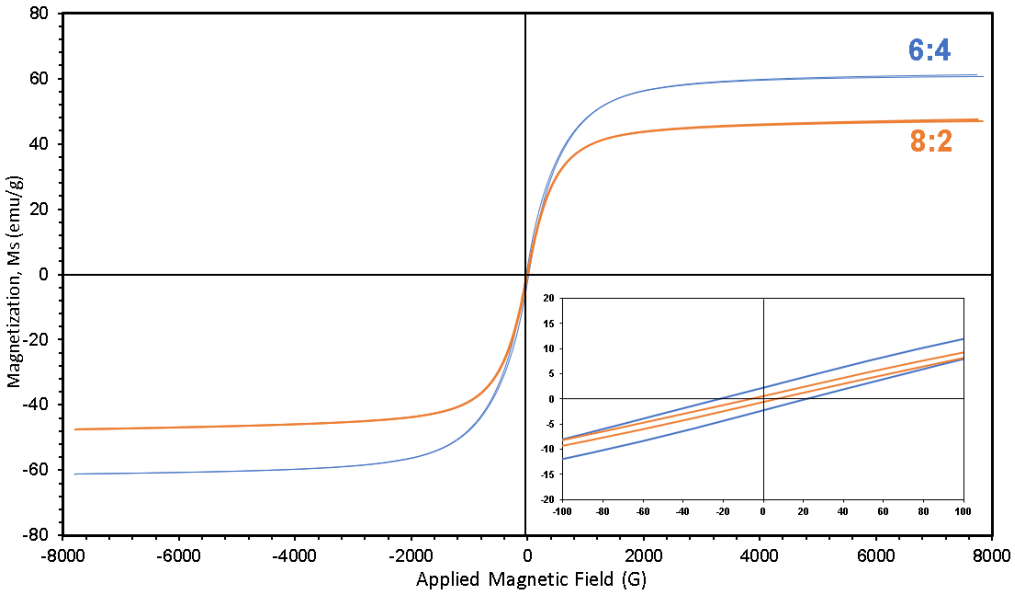

Figure 4.11: The Hysteresis Loop of the Synthesized Ni-Zn Ferrite with the Mass Ratio, $R_{(TE/N)}$ of 6:4 and 8:2.

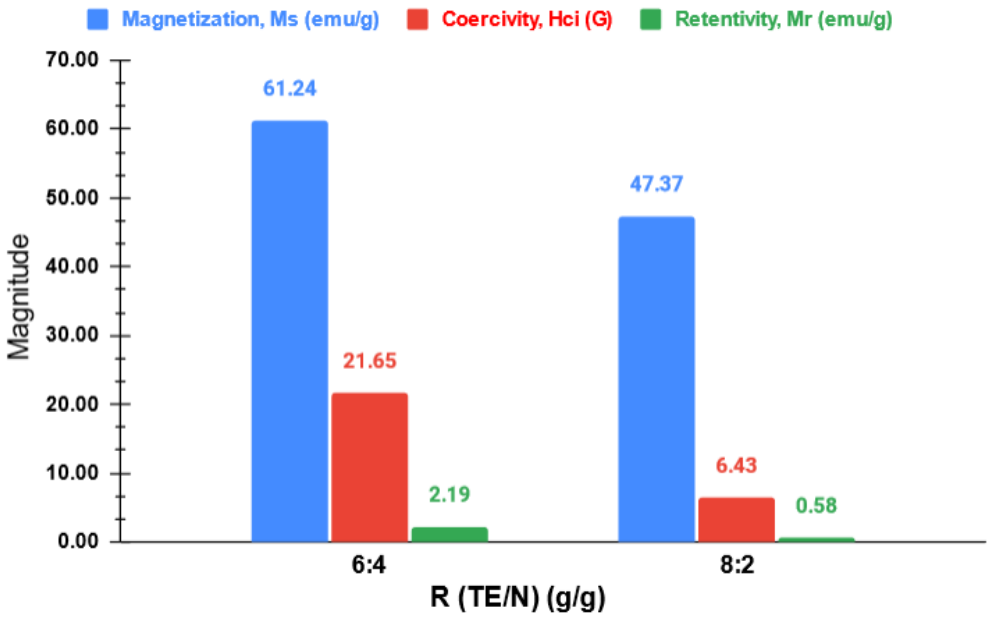

Figure 4.12: Variation of the Ms, Hci and Mr of Synthesized Ni-Zn Ferrite with the Mass Ratio, $R_{(TE/N)}$ of 6:4 and 8:2.

4.3 Summary Comparison of the Synthesized Nickel Zinc Ferrite with Other Spinel Ferrites

The magnetic performance of the synthesized nickel zinc ferrite is compared to that of the other spinel ferrites as shown in Table 4.5. Based on the comparison as shown in Table 4.5, the synthesized nickel zinc ferrite with the $R_{(TE/N)}$ of 6:4 has better magnetic performance than the synthesized nickel zinc ferrite with the $R_{(TE/N)}$ of 8:2.

Table 4.5: The List of Comparison of the Magnetic Performance Between the Synthesized Nickel Zinc Ferrite and Other Spinel Ferrites.

Spinel Ferrite (with Materials Used)	Conditions	Ms (emu/g)	Hc (Oe)	Citation
Synthesis of Ni-Zn Ferrite by Solid State Reaction from Pure Reagents				
$Ni_{0.5}Zn_{0.5}Fe_2O_4$	• Calcination temperature was 1073 K for 50 hours.	101.30	68.90	(Knyazev, et al., 2015)

(Iron (III) oxide and nickel nitrates)	• Measurement 0temperature was 3 K.			
	• Calcination temperature was 1073 K for 50 hours. • Measurement temperature was 300 K.	59.70	31.50	(Knyazev, et al., 2015)
$(Ni_{0.5}Zn_{0.5})Fe_2O_4$ (Zinc oxide, nickel (II) oxide, and iron (III) oxide)	The sintering temperature was 1250 °C for 2 hours.	83.48	24.00	(Zhao, Lv and Shen, 2009)
Synthesis of Ni-Zn Ferrite by Solid State Reaction from EAF Dust				
$(Ni,Zn)Fe_2O_4$ (ZEAFD and nickel (II) hydroxide)	The calcination temperature was 1000 °C (2 hours) and the mass ratio, $R_{ZE/N}$ was 2:0.9.	57.30	58.80	(Wang, et al., 2020)
$(Ni,Zn)Fe_2O_4$ (ZEAFD and nickel(II) chloride hexahydrate)	The calcination temperature was 1000 °C (2 hours) and the $R_{ZE/N}$ was 2:1.2.	56.80	58.50	(Wang, et al., 2017)
Synthesis of Metal(s)-Doped Zinc Ferrite				
$Mg_{1-x}Zn_xFe_2O_4$ (Iron(III) nitrate nonahydrate, magnesium nitrate hexahydrate, and zinc nitrate hexahydrate)	It was synthesized with the hydrothermal approach and the zinc content, x was 0.4.	44.50	32.70	(Tsay, Chiu and Tseng, 2019)

$Zn_{1-x}Co_xFe_2O_4$ (Iron(III) nitrate nonahydrate, cobalt(II) nitrate hexahydrate, zinc nitrate hexahydrate and sodium hydroxide)	It was synthesized with co-precipitation method and the cobalt content, x was 0.5.	82.00	75.40	(Tatarchuk, et al., 2018)
$Mn_xCo_{0.5-x}Zn_{0.5}Fe_2O_4$ (Zinc (II) nitrate hexahydrate, cobalt (II) nitrate hexahydrate, ferric (III) nitrate nonahydrate, ammonium hydroxide and citric acid anhydrous)	It was synthesized with sol-gel auto combustion method and the manganese content, x was 0.	77.31	34.63	(Mahajan, Godara and Srivastava, 2022)
	It was synthesized with sol-gel auto combustion method and the manganese content, x was 0.2.	75.30	31.31	(Mahajan, Godara and Srivastava, 2022)
Synthesized Nickel Zinc Ferrite				
$Ni_{0.5}Zn_{0.5}Fe_2O_4$ (Treated EAFD and nickel(II) chloride hexahydrate)	The sintering temperature was 1100 °C (2 hours) and the $R_{(TE/N)}$ of 6:4.	61.24	21.65	(in this project)
	The sintering temperature was 1100 °C (2 hours) and the $R_{(TE/N)}$ of 8:2.	47.37	6.43	(in this project)

CHAPTER 5

CONCLUSIONS AND RECOMMENDATIONS

5.1 Conclusion

In this project, the EAFD was used as a raw material and mixed with nickel(II) chloride hexahydrate to synthesize the nickel doped zinc ferrite. The chemical composition of the EAFD and the synthesized nickel doped zinc ferrite were determined by the EDX analysis. The franklinite, $ZnFe_2O_4$ and magnetite, Fe_3O_4 are the major phases of the EAFD. The EAFD can be treated with the diluted 0.5 mol/L of hydrochloric acid solution to synthesize a "green" magnetic material for the magnetic sensor. The nickel doped zinc ferrite ($Ni_{0.5}Zn_{0.5}Fe_2O_4$) was successfully synthesized by the solid state reaction. The calcination or sintering temperature used was 1100 °C and the time taken for the sintering process was 2 hours. The synthesized sample with the $R_{(TE/N)}$ of 6:4 has higher saturation magnetization and coercivity (61.24 emu/g and 21.65 G respectively) than the synthesized sample with the $R_{(TE/N)}$ of 8:2 (47.37 emu/g and 6.43 G respectively). Thus, the synthesized sample with the $R_{(TE/N)}$ of 8:2 has smaller hysteresis loop as compared to the synthesized sample with the $R_{(TE/N)}$ of 6:4. After comparing the magnetic performance of the synthesized samples with other spinel ferrites, the synthesized sample with the $R_{(TE/N)}$ of 6:4 is more suitable to be used as the soft magnetic material for the magnetic sensor.

5.2 Recommendations for Future Work

Lower sintering or calcination temperature should be used to synthesize the nickel zinc ferrite samples such as 800, 900 and 1000 °C. This is to evaluate the effect of the difference in the calcination temperature on the magnetic performance of the nickel zinc ferrite samples. Besides, for the EDX analysis, lead (Pb), chromium (Cr), and cadmium (Cd) must be inspected for the EAFD, treated EAFD and the synthesized samples. This is because the EAFD is considered hazardous due to the presence of these 3 elements. The synthesized samples should not contain them as they will affect the quality of the synthesized nickel zinc ferrite sensor material detrimentally. In addition, the ICP-OES which stands for Inductively Coupled Plasma - Optical Emission Spectrometry can be

utlised to examine the composition of the filtrate solution from the EAFD treatment process. This can indicate the amount of certain elements that have been removed by the HCl solution during the treatment process. Furthermore, during the treatment of the EAFD process, there is a precaution step for the solid-liquid separation process. When the mixture is filtered, it is best to collect all the solids in the same filter paper. This is to prevent mass loss of the collected treated EAFD in the filter paper. In addition, fluted filter paper is suggested to be used for the treatment process instead of conical filter paper. This is because the fluted filter paper has larger surface area than the conical filter paper. Thus, large surface area results in faster filtration process.

REFERENCES

Academy of Sciences Malaysia, 2020. *10-10 MALAYSIAN SCIENCE, TECHNOLOGY, INNOVATION AND ECONOMY (MYSTIE) FRAMEWORK*. Kuala Lumpur: Academy of Sciences Malaysia.

Asfour, A. ed., 2017. *Magnetic Sensors: Development Trends and Applications*. BoD–Books on Demand.

Babu, B.R. and Tatarchuk, T., 2018. Elastic properties and antistructural modeling for nickel-zinc ferrite-aluminates. Materials Chemistry and Physics, 207, pp.534-541.

Berthomieu, C. and Hienerwadel, R., 2009. Fourier transform infrared spectroscopy. *Photosynthesis Research*, 101(2–3), pp. 157–170.

Cal Poly Pomona, 2021. Infrared Tables (short summary of common absorption frequencies). [online] Available at: <https://www.cpp.edu/~psbeauchamp/pdf/spec_ir_nmr_spectra_tables.pdf> [Accessed 18 April 2022].

Chairaksa-Fujimoto, R., Maruyama, K., Miki, T. and Nagasaka, T., 2016. The selective alkaline leaching of zinc oxide from Electric Arc Furnace dust pre-treated with calcium oxide. *Hydrometallurgy*, *159*, pp.120-125.

de Buzin, P.J.W.K., Heck, N.C. and Vilela, A.C.F., 2017. EAF dust: An overview on the influences of physical, chemical and mineral features in its recycling and waste incorporation routes. *Journal of materials research and technology*, 6(2), pp.194-202.

Džunuzović, A.S., Ilić, N.I., Petrović, M.V., Bobić, J.D., Stojadinović, B., Dohčević-Mitrović, Z. and Stojanović, B.D., 2015. Structure and properties of Ni–Zn ferrite obtained by auto-combustion method. *Journal of Magnetism and Magnetic Materials*, 374, pp.245-251.

Fair-Rite Products Corp., 2021. *Ferrite Components for the Electronic Industry*. [online] Available at: <http://www.fair-rite.com/files1/Fair-Rite_Catalog_17th_Edition.pdf > [Accessed 1 September 2021].

Gao, J.M. and Cheng, F., 2018. Effect of metal substitution on the magnetic properties of spinel ferrites synthesized from zinc-bearing dust. *Journal of Superconductivity and Novel Magnetism*, 31(7), pp.1965-1970.

Guézennec, A.G., Huber, J.C., Patisson, F., Sessiecq, P., Birat, J.P. and Ablitzer, D., 2005. Dust formation in electric arc furnace: birth of the particles. *Powder technology*, 157(1-3), pp.2-11.

Kaur, A. and Bhargava, G.K., 2021. Review paper on nickel-zinc nano ferrite. *Materials Today*: Proceedings, 37, pp.3082-3086.

Knyazev, A.V., Zakharchuk, I., Lähderanta, E., Baidakov, K.V., Knyazeva, S.S. and Ladenkov, I.V., 2017. Structural and magnetic properties of Ni-Zn and Ni-Zn-Co ferrites. *Journal of Magnetism and Magnetic Materials*, 435, pp.9-14.

Kumbhar, S.S., Mahadik, M.A., Mohite, V.S., Rajpure, K.Y., Kim, J.H., Moholkar, A.V. and Bhosale, C.H., 2014. Structural, dielectric and magnetic properties of Ni substituted zinc ferrite. *Journal of magnetism and magnetic materials*, 363, pp.114-120.

Kurian, M. and Nair, D.S., 2016. Effect of preparation conditions on nickel zinc ferrite nanoparticles: a comparison between sol–gel auto combustion and co-precipitation methods. Journal of Saudi Chemical Society, 20, pp.S517-S522.
Mahajan, H., Godara, S.K. and Srivastava, A.K., 2022. Synthesis and investigation of structural, morphological, and magnetic properties of the manganese doped cobalt-zinc spinel ferrite. *Journal of Alloys and Compounds*, *896*, p.162966.

Moradpour, Z., Taghavi, S.H., Hesam, G., Atamaleki, A. and Garkaz, A., 2020. Investigation of Dust Chemical Compounds Emitted by Electric Arc Furnace (EAF) with a reuse perspective. *Iranian Journal of Health*, Safety and Environment, 7(1), pp.1408-1412.

Nezhad, S.M. and Zabett, A., 2016. Thermodynamic analysis of the carbothermic reduction of electric arc furnace dust in the presence of ferrosilicon. *Calphad*, *52*, pp.143-151.

Qin, H., He, Y., Xu, P., Huang, D., Wang, Z., Wang, H., Wang, Z., Zhao, Y., Tian, Q. and Wang, C., 2021. Spinel ferrites (MFe2O4): Synthesis, improvement and catalytic application in environment and energy field. *Advances in Colloid and Interface Science*, p.102486.

Rieger, J., Colla, V., Matino, I., Branca, T.A., Stubbe, G., Panizza, A., Brondi, C., Falsafi, M., Hage, J., Wang, X. and Voraberger, B., 2021. Residue Valorization in the Iron and Steel Industries: Sustainable Solutions for a Cleaner and More Competitive Future Europe. *Metals*, *11*(8), p.1202.

Simonyan, L.M., Alpatova, A.A. and Demidova, N.V., 2019. The EAF dust chemical and phase composition research techniques. *Journal of Materials Research and Technology*, 8(2), pp.1601-1607.

Tatarchuk, T.R., Paliychuk, N.D., Bououdina, M., Al-Najar, B., Pacia, M., Macyk, W. and Shyichuk, A., 2018. Effect of cobalt substitution on structural, elastic, magnetic and optical properties of zinc ferrite nanoparticles. *Journal of Alloys and Compounds*, *731*, pp.1256-1266.

Thakur, P., Taneja, S., Chahar, D., Ravelo, B. and Thakur, A., 2021. Recent advances on synthesis, characterization and high frequency applications of Ni-Zn ferrite nanoparticles. *Journal of Magnetism and Magnetic Materials*, p.167925.

Tsay, C.Y., Chiu, Y.C. and Tseng, Y.K., 2019. Investigation on structural, magnetic, and FMR properties for hydrothermally-synthesized magnesium-zinc ferrite nanoparticles. *Physica B: Condensed Matter*, 570, pp.29-34.

Wang, H.G., Gao, J.M., Liu, W., Zhang, M. and Guo, M., 2016. Recovery of metal-doped zinc ferrite from zinc-containing electric arc furnace dust: Process development and examination of elemental migration. *Hydrometallurgy*, 166, pp.1-8.

Wang, H.G., Li, J.W., Huo, X.T., Yue, C.S., Peng, B., Zhang, M. and Guo, M., 2020. Magnetic Ni-Zn spinel ferrite nanopowder from toxic Zn-bearing electric arc furnace dust: A promising treatment process. *Minerals Engineering*, 157, p.106540.

Wang, H.G., Guo, M. and Zhang, M., 2017. Direct Preparation of Metal Doping Ni–Zn Ferrite from Zn-Containing Electric Arc Furnace Dust by Calcination Method. In *Energy Technology 2017* (pp. 191-201). Springer, Cham.

Wang, H.-gang, Zhang, M. and Guo, M., 2017. Utilization of zn-containing electric arc furnace dust for multi-metal doped ferrite with enhanced magnetic property: From hazardous solid waste to green product. *Journal of Hazardous Materials*, 339, pp.248–255.

World Steel Association, 2018. *Steel industry co-products*. Belgium: World Steel Association.

Xiaobin, W.A.N.G., Xiuying, L.I., Xiang, Y.A.N., Cheng, T.U. and Zhaoguo, Y.U., 2021. Environmental risks for application of iron and steel slags in soils in China: A review. *Pedosphere*, 31(1), pp.28-42.

Yoo, J.M., Kim, B.S., Lee, J.C., Kim, M.S. and Nam, C.W., 2005. Kinetics of the volatilization removal of lead in electric arc furnace dust. *Materials transactions*, *46*(2), pp.323-328.

Zhao, D.L., Lv, Q. and Shen, Z.M., 2009. Fabrication and microwave absorbing properties of Ni–Zn spinel ferrites. *Journal of Alloys and Compounds*, 480(2), pp.634-638.